https://doi.org/10.1016/j.trb.2019.04.010



# Capacity Approximations for Near- and Far-side Bus Stops in Dedicated Bus Lanes

Minyu Shen[a], Weihua Gu[a*], Sangen Hu[a,b], and Han Cheng[c]

[a]Department of Electrical Engineering, The Hong Kong Polytechnic University
[b]School of Civil and Transportation Engineering, Guangdong University of Technology, China
[c]Department of Civil and Environmental Engineering, University of California, Berkeley

## Abstract

We develop analytical approximations for the bus-carrying capacities at near- and far-side stops with one or multiple curbside berths where buses operate in a dedicated bus lane. The approximations are derived using time-space diagrams of bus trajectories and probabilistic methods. They correctly account for the effects of key operating factors that were ignored or incorrectly addressed by previous methods. These factors include the signal timing and the distance between stop and signal. Comparison against computer simulation shows that our models furnish much more accurate estimates for near- and far-side stop capacities than previous methods in the literature. Numerical case studies are performed to examine how the stop capacity is affected by various operating factors. New findings and their practical implications are discussed.

**Keywords:** bus-stop capacity; near-side bus stops; far-side bus stops; bus queues; tandem queues

## 1 Introduction

Transit management agencies often place bus stops near signalized intersections to facilitate passengers' access via protected street crossings (Fitzpatrick et al., 1996). Figures 1a and b illustrate the two types of these stops, which are termed according to whether the stop is placed at the near-side (i.e. upstream side) or far-side (i.e. downstream side) of the intersection. On the other hand, the bus-carrying capacities of these stops will be curbed by the neighboring traffic signal. As a result, long bus queues often form at busy stops of this kind during rush hours (Gibson, 1996; Tan and Yang, 2014). The bus queues will cause multifarious negative impacts, including large delays to bus passengers, poor bus schedule reliability, and blockage of the adjacent traffic.

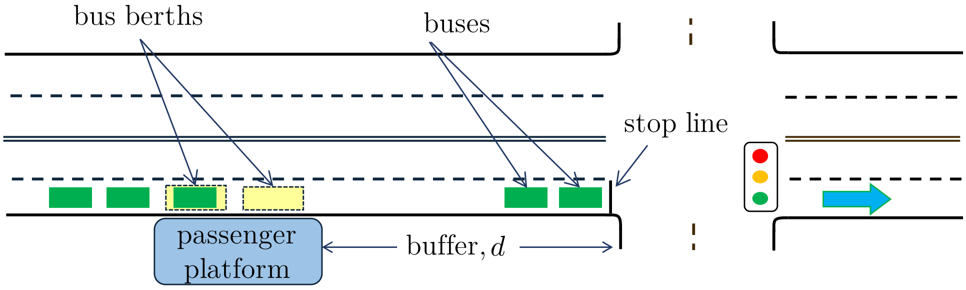


(a) A near-side stop

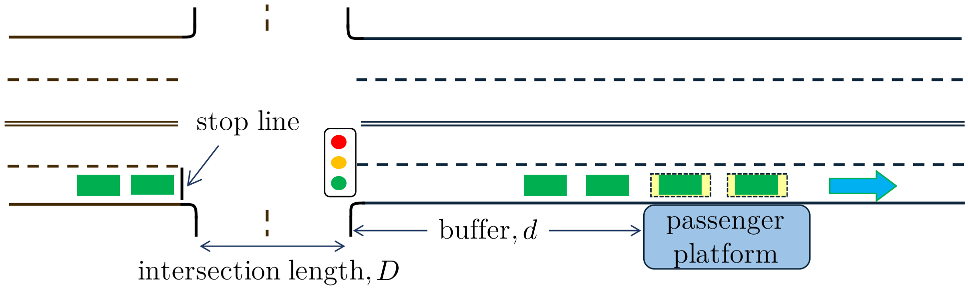


(b) A far-side stop

Figure 1: Curbside bus stops near signalized intersections.

To avoid the ever-expanding bus queues, the transit agency needs to properly determine a stop's layout (including the number of berths) and location such that the maximum estimated bus arrival rate does not exceed the stop's bus-carrying capacity. To this end, formulas and methods for estimating the capacities for near- and far-side stops have been furnished in the literature. The best-known capacity formula was first presented by the Highway Capacity Manual (HCM: TRB, 2000), and was later inherited by the Transit Capacity and Quality of Service Manual (TCQSM: Kittelson & Associates, Inc., 2013). The latest version of this formula (Equation 6-18 of TCQSM) is:

$$B_s = N_{el} f_{tb} \frac{3600(G/C)}{t_c + t_d(G/C) + Z c_v t_d}, \tag{1}$$

where $B_s$ denotes the stop capacity; $N_{el}$ the effective number of berths, which accounts for the mutual blockage between the buses dwelling in multiple, tandemly deployed berths; $f_{tb}$ the traffic blockage adjustment factor to account for the impacts of competing (right- or left-turning) traffic in the travel lane of buses; $G/C$ the green ratio of the neighboring traffic signal with $G$ being the green period and $C$ the cycle length; $t_c$ is the clearance time, which includes a bus's movement time in and out of a berth and its "re-entry delay" for merging back to the general traffic from a bus bay; $t_d$ a bus's dwell time for loading and unloading passengers; and $Z c_v t_d$ the so-called "operating margin" that accounts for the randomness in bus dwell time.

This formula is known to have a number of serious flaws, including the abuse of the empirical, site-specific values for $N_{el}$ (see Exhibit 6-63 in TCQSM), and the fallacious derivation regarding the operating margin term. Those problems have been reported by Gu et al. (2011, 2015) and Gu (2012), and the details are omitted here in the interest of brevity. Moreover, the way for modeling the effect of the neighboring traffic signal in equation (1) is also questionable. First, the equation simply discounts both the numerator and the bus dwell time $t_d$ in the denominator by the signal's green ratio. This oversimplified the effect of signal timing on the stop capacity, and ignored the effect of signal cycle length on the capacity given a fixed green ratio. (We will see momentarily in this paper that cycle length has a significant impact on the stop capacity even when green ratio is fixed.) Second, the equation presumes that the effect of multiple berths on the stop capacity, represented by the coefficient $N_{el}$, is multiplicative and independent of the effect of signal. And lastly, the equation totally overlooked how the stop capacity would be affected by the distance between the stop and its neighboring signal. A recent modification of (1) was reported by Hisham et al. (2018), which still did not solve any of the above problems.

Other studies also reported some of these problems (Gibson, 1996; Fernández et al., 2007; Fernández, 2010; Cortés et al., 2010; Tan and Yang, 2014). Some of those works proposed hypothetical models as replacement of (1). These models were calibrated by site-specific data, and thus they are only applicable to a narrow range of sites. Other studies relied on simulations that can capture more realistic features of bus stop operations. However, simulations are "blackboxes" that cannot readily reveal general insights on cause-and-effect relationship between key operating parameters and stop capacity. Many simulations are also computationally more demanding, and thus may not be suitable for investigating a large number of cases under various operating environments. In addition, practitioners always desire to have a simple formula, or recipe to be used conveniently. Such a formula or recipe cannot be obtained by regressing empirical or simulated data to some hypothetical function forms, because the stop capacity is a complicated function of several key input parameters, including the number of berths, the distance between stop and signal, the signal timing (cycle length and green ratio), and the distribution of bus dwell times.

Analytical queuing models, on the other hand, are capable of describing the causal relationships between the stop capacity and key input parameters. These models are also more computationally efficient, and are often used to unveil general insights by examining large batches of numerical instances. For example, Markovian methods were often used to develop exact solutions to queuing models with tandemly-deployed servers, e.g. a multi-berth stop that is isolated from the influence of nearby signals (Gu et al., 2012, 2015; Gu and Cassidy, 2013; Bian et al., 2019). Unfortunately, the above methods cannot be extended to solve the near- and far-side stop queuing models, because these queuing models integrate two types of servers: tandemly-deployed berths and the traffic signal, and the latter is not Markovian (Newell, 1965). Hence exact solutions to these queuing models are difficult to obtain. When exact analytical solution is unavailable, approximations are often sought instead (e.g., Newell, 1965, 1982; Whitt, 1993; Gross et al., 2008).

In light of the above, we develop parsimonious approximations for near- and far-side stops' capacities under various operating conditions. For simplicity, we consider only curbside stops where: i) bus maneuvers are restricted within the curbside travel lane, which is dedicated to bus use only[1]; ii) buses are not allowed to overtake each other at the stop or the intersection, or in any queue that forms upstream of the stop or intersection[2]; iii) for a near-side stop, buses that are ready to depart the stop but are blocked by the red signal are all able to discharge during the following green phase; and iv) for a far-side stop, the empty berths and the buffer space between stop and signal (see Figure 1b) can all be filled up by buses discharging through the intersection in a green phase, should a bus queue be always present upstream of the intersection[3].

Our approximations correct the flaws of the TCQSM formula by properly accounting for the effects on stop capacity from all the key operating factors mentioned above. Validations via computer simulation show that the approximations exhibit quite good accuracy. A number of managerial insights are also unveiled from extensive numerical case studies.

The approximation models are presented in Section 2. Validation tests are furnished in Section 3, together with a comparison against the TCQSM formula. Numerical examples are discussed in Section 4. Insights stemming from our models and their practical implications are described in Section 5.

# 2 Approximations for near- and far-side stop capacities

We consider near- and far-side bus stops like those shown in Figures 1a and b, where the number of berths is denoted by $c$. The land area between the stop and the intersection is termed as "buffer area", whose size is denoted by the (integer) number of buses that can reside within, $d$, as illustrated in the figures. If the buffer size is not an integer multiple of berth length, it will be rounded down to the nearest smaller integer since only an integer number of buses can be stored in the buffer. We further write $d$ as the sum of an integer multiple of $c$ and a non-negative residual: $d = nc + d_0$, where $n = 0, 1, 2, ...,$ and $0 \leq d_0 \leq c - 1$. We define a bus's dwell time, $S$, as the sum of: i) the time for loading and unloading passengers in a berth; ii) the time lost due to bus deceleration and acceleration; and iii) the time lost due to door opening and closing. We assume that dwell times of different buses are independent and identically

[1] At some busy stops not residing in a bus lane, bus operations may still enjoy a "de facto" exclusive right-of-way since other traffic often stay away from the neighborhood of those busy stops to avoid being blocked by the slow-moving and large-sized buses (Gibson et al., 1989; Fernandez and Planzer, 2002). The models to be presented in this paper can still be applied to those stops with caution.

[2] This assumption represents a common type of bus-stop operation rules (St. Jacques and Levinson, 1997; Kittelson & Associates, Inc., 2013). The same assumption was also made in other studies in this realm (Gu et al., 2011, 2015; Bian et al., 2015).

[3] Assumptions iii) and iv) are practically valid in general as explained below. For near- and far-side stops in the real world, the distance between the stop and the intersection is usually less than 100 meters and so can store at most 8 buses (suppose bus jam spacing is 12 meters). A stop located 100 meters away from the intersection can be regarded as a mid-block stop (Kittelson & Associates, Inc., 2013), on which the signal has a small impact. Moreover, stops with more than 4 berths are rare. Even for the extreme case of a 4-berth stop located 100 meters from the nearby intersection, to satisfy assumptions iii) and iv), the green period only needs to be long enough to discharge 12 buses consecutively. This requires a 42-second green period given a saturation headway of 3.5 seconds for discharging buses (Nguyen, 2013). A signal timing plan with more than 42 seconds green time is commonly used, especially at major intersections where neighboring stops are often congested.

distributed (i.i.d.) with mean $\mu_S$ and coefficient of variation $C_S$.[4] The signal cycle length and effective green period are denoted as $C$ and $G$, respectively. Without loss of generality, we normalize all the time variables, unless otherwise specified, by setting the mean bus dwell time as the unit time, i.e., $\mu_S = 1$. We also normalized all the distance variables by setting the berth length (or equivalently, the bus jam spacing) as the unit distance. These normalizations will largely simplify the derivation of approximations.

To derive the bus stop capacity (i.e., the maximum bus discharging rate from a stop), we specify that a bus queue is always present upstream of a near-side stop, or upstream of the intersection for the far-side stop case. Under this condition, assumptions iii) and iv) in the previous section mean that the green period is long enough for at least $d + c$ buses to discharge consecutively into the intersection, given that they are ready to discharge at the start of the green signal.

The approximation models for near-side stops are developed in Section 2.1. Those for far-side stops are developed in Section 2.2. The notations used in this paper are summarized in Appendix A.

## 2.1 Near-side stop models

We first develop the capacity approximations for a single-berth near-side stop (Section 2.1.1) since in this simple case our key idea for constructing the approximation can be presented more clearly. The single-berth stop approximation is then built upon to develop the approximation for multi-berth stops in Section 2.1.2.

### 2.1.1 Capacity approximation for a single-berth near-side stop ($c = 1$ and $d = n$)

The downstream signal affects the stop's capacity only when a queue of buses formed at the intersection during a red period spills back to the berth, so that the berth cannot serve new buses. We denote $T_B$ as the time during which the berth is blocked in a cycle. The single-berth near-side stop's capacity, $Q_S$, can then be written as:

$$Q_S = \frac{1}{1 + \tau_m} \left( 1 - \frac{E[T_B]}{C} \right), \tag{2}$$

where $\tau_m$ is a bus's movement time in and out of a berth (i.e., the clearance time $t_c$ in equation (1) for curbside stops). The $\frac{1}{1+\tau_m}$ is the capacity of an isolated single-berth stop (i.e., a stop without neighboring signals), since the denominator is the sum of average dwell time (note $\mu_S = 1$) and the average time a bus takes to move forward and fill the berth after the previous bus has left. The remaining work is on how to approximate $E[T_B]$.

[4]One may also find more complicated bus dwell time models, which account for how passengers are loaded to and unloaded from a bus in, e.g., Jaiswal et al. (2010) and Fernández et al. (2008). However, for the simplicity of our modeling work, we adopt the present assumption that the bus dwell times are i.i.d. The same assumption has also been commonly used in the literature; see TCQSM (2013) and Gu et al. (2011, 2015).

To find $E[T_B]$, we first define the "extended red period" at the berth's location, during which buses can be served, but cannot discharge into the intersection. This extended red period is illustrated in the time-space diagrams of bus trajectories at a single-berth near-side stop; see Figure 2 for the case of $d = n = 3$. The solid lines with arrowheads in the figures represent trajectories of the *front* of buses, and the thicker, horizontal segments (labeled as $S_1$, $S_2$, $S_3$ and $S_4$) of these trajectories represent bus dwell times. In the interest of brevity, these trajectories are plotted as piecewise linear curves; see, e.g., Gu et al. (2013, 2014) for studies that also use piece-wise linear vehicle trajectories for analysis.

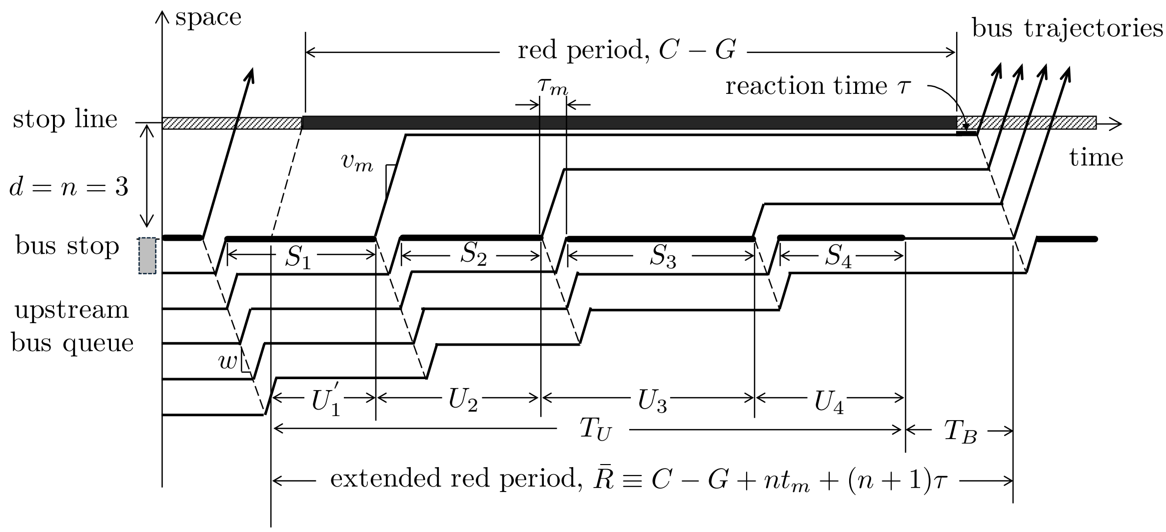


Figure 2: Time-space diagram of bus operations at a single-berth near-side stop ($d = n = 3$).

As illustrated in Figure 2, the extended red period starts $\frac{n}{v_m}$ earlier than a red period, and ends $\frac{n+1}{w}$ later than the same red period, where $v_m$ is the bus's move-up speed when traveling through the queue, the berth and the buffer, and $w$ is the backward wave speed of bus traffic.[5] For the convenience of description, we denote $\tau = \frac{1}{w}$ (which is termed the "reaction time" in some literature; see for example Menendez, 2006) and $t_m = \frac{1}{v_m}$. (Note that $\tau_m = \tau + t_m$.) Hence, the duration of extended red period is $\bar{R} \equiv C - G + nt_m + (n+1)\tau$, as shown in Figure 2. Note that assumption iii) ensures that $G \geq (c + d)\tau_m$, hence the extended red period will never exceed the cycle length.

The start time of extended red period is determined such that any bus that finishes service before this start time will be able to discharge into the intersection immediately. On the other hand, the dwelling bus at this start time and all the following buses served during this extended red period will have to wait until the next green period to discharge; see Figure 2. The number of these trapped buses is no greater than the storage capacity of the berth and the buffer, i.e., $n + 1$ (= 4 in Figure 2). The last trapped bus (regardless of the number of trapped buses) will depart the berth no earlier than $(n + 1)\tau$ after the green start, and this time defines the end of the extended red period, as illustrated again in Figure 2. If $n + 1$ buses are served

[5]The backward wave speed is the speed at which the disturbances (in our case, the change of bus speed) propagate backwardly across the buses (Newell, 1993; Daganzo, 1994).

in an extended red period, a blocked duration $T_B > 0$ may exist at the end of extended red period (see again the case of Figure 2); otherwise, the berth is busy throughout the extended red period and $T_B = 0$.

Figure 2 also shows that $T_B$ can be calculated by:

$$T_B = max\{\bar{R} - T_U, 0\}, \tag{3}$$

where $T_U$ denotes the sum of dwell times of the $n+1$ consecutive buses served in the extended red period plus their reaction and move-up times. It can be written as follows:

$$T_U = U_1^{'} + \sum_{j=2}^{n+1} U_j, \tag{4}$$

where $U_1^{'}$ denotes the portion of the first trapped bus's dwell time that is contained in the extended red period; and $U_j = S_j + \tau_m$ $(j = 2, 3..., n+1)$ (see again Figure 2).

We can derive from equation (3) that:

$$E\left[T_B\right] = \int_{t=0}^{\bar{R}} (\bar{R} - t) f_{T_U}(t) dt, \tag{5}$$

where $f_{T_U}(t) = \left(f_{U_1'} * \underbrace{f_U * ... * f_U}_{n\ times}\right)(t)$ is the probability density function (PDF) of $T_U$; $f_{U_1'}$ and $f_U$ are the PDFs of $U_1^{'}$ and $U_j$ respectively, and the "$*$" is the convolution operator.

We now approximate $T_U$ by a normal random variable with the same mean $\mu_T$ and variance $\sigma_T^2$. For large $n$'s, this normal approximation is quite accurate thanks to the central limit theorem (CLT). But even for a relatively small $n$, the approximation can be fairly good. This is because: i) most of the components in the right hand side of (4), i.e. the $U_j$'s $(j = 2, 3, ..., n+1)$ are i.i.d and usually exhibit a bell-shaped PDF in the real world; and ii) although $U_1^{'}$ has a different distribution from $U_j$, it is statistically smaller than $U_j$ and thus has a small share in $T_U$ if $n$ is not too small. On the other hand, this CLT approximation may be less accurate if $n = 0$ or 1.

Applying the properties of normal distribution, we have:

$$\begin{aligned}
E\left[T_B\right] &= \bar{R} F_{T_U}(\bar{R}) - \int_{t=0}^{\bar{R}} t f_{T_U}(t) dt \\
&= \bar{R} F_{T_U}(\bar{R}) - \int_{t=-\infty}^{\bar{R}} t f_{T_U}(t) dt \\
&\approx \bar{R} \Phi\left(\frac{\bar{R} - \mu_T}{\sigma_T}\right) - \left(\mu_T \Phi\left(\frac{\bar{R} - \mu_T}{\sigma_T}\right) - \sigma_T \phi\left(\frac{\bar{R} - \mu_T}{\sigma_T}\right)\right) \\
&= \sigma_T (r \Phi(r) + \phi(r)),
\end{aligned} \tag{6}$$

where $F_{T_U}(\cdot)$ denotes the cumulative distribution function (CDF) of $T_U$; $\Phi(\cdot)$ and $\phi(\cdot)$ the CDF and PDF of a standard normal distribution, respectively; and $r = \frac{\bar{R}-\mu_T}{\sigma_T}$. The second equality in (6) holds because $T_U$ is non-negative. The approximation step in (6) is obtained as follows: first approximate $f_{T_U}(t)$ by the PDF of a normal distribution with mean $\mu_T$ and variance $\sigma_T^2$ (the CLT approximation), and then apply the mean formula of a truncated normal distribution whose lower and upper truncated bounds are $-\infty$ and $\bar{R}$, respectively (see e.g., Greene, 2003).

Combining equations (2) and (6) furnishes an approximation of the single-berth stop's capacity, denoted as $Q_{SA}$:

$$Q_{SA} = \frac{1}{1+\tau_m}\left(1 - \frac{\sigma_T(r\Phi(r) + \phi(r))}{C}\right). \tag{7}$$

Finally, when $S_j$ follows a gamma distribution[6], the mean $\mu_T$ and variance $\sigma_T^2$ of $T_U$ are approximated as follows:

$$\begin{cases} \mu_T \approx n(1+\tau_m) + \dfrac{C_S^2 + (1+\tau_m)^2}{2(1+\tau_m)}; \\ \sigma_T^2 \approx \dfrac{5+8\tau_m}{12(1+\tau_m)^2} C_S^4 + (\dfrac{1}{2}+n)C_S^2 + \dfrac{(1+\tau_m)^2}{12}. \end{cases} \tag{8}$$

The derivation of (8) is relegated to Appendix B.

Approximation (7) exhibits high accuracy when $n$ is large. But moderate errors may occur when $n$ is rather small. Fortunately, our numerical results manifest that the accuracy of (7) is fairly good even when $d = 0$; see Section 3.1 for more details.

Significant errors may also occur when $C_S$ is small, since (8) is derived using an assumption that $U_1'$ is independent of signal phases (see Appendix B), which becomes invalid for small $C_S$. An extreme example where $C_S = 0$ (deterministic bus dwell time) is briefly discussed in Appendix B. More details regarding the accuracy of (7) are furnished in Section 3.

### 2.1.2 Capacity approximation for a multi-berth near-side stop ($c \geq 2$ and $d = nc + d_0$)

Since bus overtaking maneuvers are prohibited, the bus dwelling at the upstream-most berth of a multi-berth stop can depart only when all the downstream berths are vacated. Thus, in the absence of the traffic signal, queued buses will enter a $c$-berth curbside stop in convoys of size $c$ (Gu et al., 2011), should a sufficiently long bus queue be present all the time. We denote $U^p$ as the general service time of a $c$-bus convoy, which is defined as the total time the convoy spends at the $c$-berth stop for all of its buses to finish dwelling. Then a $c$-bus convoy served at a $c$-berth stop can be viewed as a hypothetical "bus" that spends a random "dwell time", $U^p$,

[6]Gamma distribution fits the real-world bus dwell times well (see, e.g., Ge, 2006), and was often used to model bus dwell times in the literature due to its non-negativity, parsimony and flexibility (Gu et al., 2011; Gu and Cassidy, 2013). However, our method can still be used if the bus dwell time is assumed to follow other commonly used distributions, e.g. the log-normal distribution (Wang et al., 2016, 2018).

at a "single-berth" stop. The distribution of $U^p$ can be developed using the probability theory. Specifically, we find that the mean and variance of $U^p$ can be approximated by the following functions (assuming $S$ follows gamma distribution):

$$\begin{cases} E[U^p] \approx h(c, C_S) \equiv 0.7931 C_S \log(c) + 0.9911 + c\tau_m; \\ Var(U^p) \approx q(c, C_S) \equiv 0.6819 C_S^3 \arctan(c) + 0.5102 C_S^2. \end{cases} \tag{9}$$

The derivation of (9) is relegated to Appendix C. The appendix also includes a test of the accuracy of (9).

We now follow the logic in Section 2.1.1 to develop the approximate capacity; i.e., we consider that a $c$-berth stop's capacity ($c \geq 2$) is equal to the capacity of an isolated $c$-berth stop, multiplied by the fraction of time when the stop is not blocked by the queue arising from the signal. The blockage of the stop is again determined with the assistance of an extended red period, which is now defined at the location of the upstream-most berth with a duration of $\bar{R}^p \equiv C - G + (c + d - 1)t_m + (c + d)\tau$; see Figure 3 for a 2-berth, 2-buffer stop as an example.

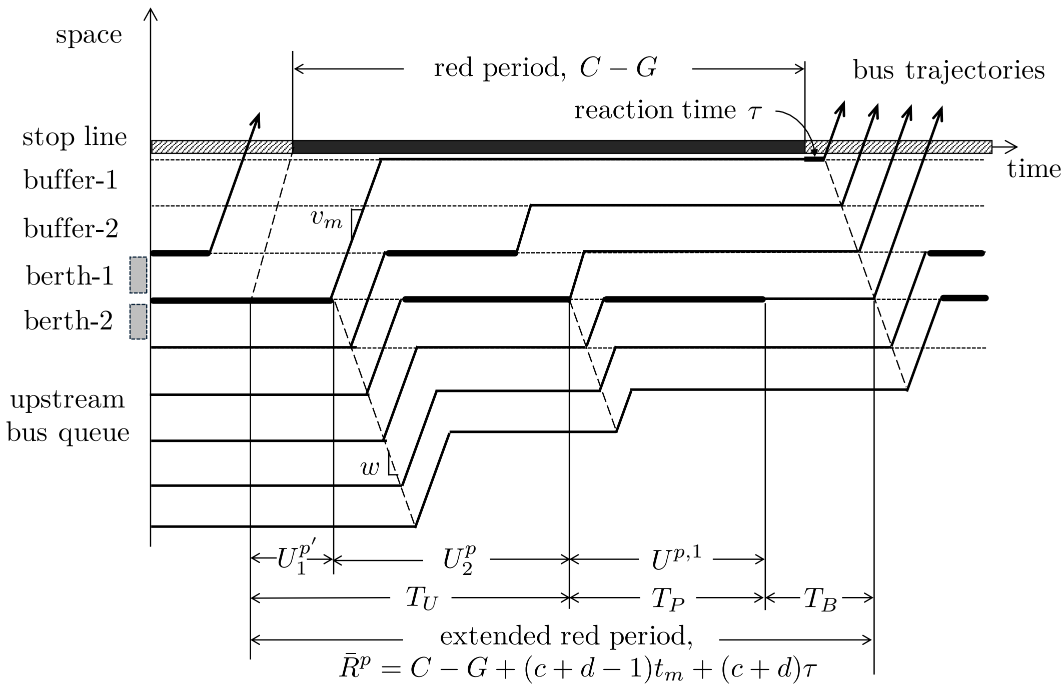


Figure 3: Time-space diagram of bus operations at a 2-berth, 2-buffer near-side stop.

For a multi-berth stop, the number of available buffer spaces near the end of an extended red period may be greater than 0 but less than $c$. In this case, only part of the $c$-bus convoy that is currently under service can proceed to the buffer after completing the services. The remaining buses in the convoy have to stay at the downstream berths of the stop. Consequently, the next bus convoy to be served by the stop would contain fewer than $c$ buses. In the example shown in Figure 3, the last "convoy" served in the extended red period has only one bus. With a slight abuse of notation, we use the same symbol $T_U$ (as in the single-berth case) to denote the part of extended red period for serving part of the first trapped convoy and all the *full*-size convoys. We denote $T_P$ as the time for serving the last *small* convoy if any, and $T_B$ as the time interval when all the berths are occupied by buses waiting for departure (i.e., when the stop is effectively idle). The $T_U$, $T_P$ and $T_B$ are illustrated in Figure 3. The stop's service rate is 0 during $T_B$, and is discounted by $1 - \frac{N_P}{c}$ during $T_P$, where $N_P$ is the number of buses in the small convoy. For simplicity, we further define the "effective service time of full-size convoys" as $T_U' = T_U + \frac{N_P}{c} T_P$, and the "effective blockage time" as $T_B' = max\{\bar{R}^p - T_U', 0\}$. We then write the approximate stop capacity as:

$$Q_{MA} \approx \left(\frac{c}{E[U^p]}\right)\left(1 - \frac{E[T_B']}{C}\right). \tag{10}$$

Note that (10) is an analog of (2) in the single-berth case. Following a derivation similar to the CLT approximation in Section 2.1.1, we have the approximate stop capacity:

$$Q_{MA} = \left(1 - \frac{\sigma_{T_U'}(r\Phi(r) + \phi(r))}{C}\right)\left(\frac{c}{h(c, C_S)}\right), \tag{11}$$

where $r = \frac{\bar{R}^p - \mu_{T_U'}}{\sigma_{T_U'}}$, $\mu_{T_U'}$ and $\sigma_{T_U'}$ are mean and standard deviation of $T_U'$.

Finally, $\mu_{T_U'}$ and $\sigma^2_{T_U'}$ are approximated by (again, assuming $S$ follows gamma distribution):

$$\begin{cases} \mu_{T_U'} \approx (n + \frac{1}{2})h(c, C_S) + \dfrac{q(c, C_S)}{2h(c, C_S)} + \dfrac{c + d_0 - E[M]}{c} h(c + d_0 - E[M], C_S); \\ \sigma^2_{T_U'} \approx \dfrac{1}{12} h^2(c, C_S) + (n + \frac{1}{2}) q(c, C_S) + \dfrac{5h(c, C_S) + 3\tau_m}{12h^2(c, C_S)(h(c, C_S) - c\tau_m)} q^2(c, C_S) \\ \qquad + \left(\dfrac{c + d_0 - E[M]}{c}\right)^2 q(c + d_0 - E[M], C_S). \end{cases} \tag{12}$$

Derivation of (12) is relegated to Appendix D.

## 2.2 Far-side stop models

The approximations for far-side stops are derived in similar ways as for near-side stops. The major difference lies in the calculation of the idle time period: a far-side stop becomes idle when the stop is starved by the upstream red signal, which cuts off the bus inflow. We again present the approximation for single-berth stops first (in Section 2.2.1) to smooth the reading experience, and then for the more complicated multi-berth stops in Section 2.2.2. In both sections, we denote $D$ as the length of intersection, i.e., the distance between stop line and the start of buffer; see Figures 1b, 4a and 4b.

### 2.2.1 Capacity approximation for a single-berth far-side stop ($c = 1$ and $d = n$)

We first define the extended red period, again at the berth's location, as shown by the example of a far-side single-berth stop with $d = 2$ (Figure 4a). It starts from the black dot on the left, which is $(n + 1)\tau$ ahead of the red start, and ends at the grey point on the right, which is $(D+n)t_m$ later than the following green start. The two dots are determined using the following

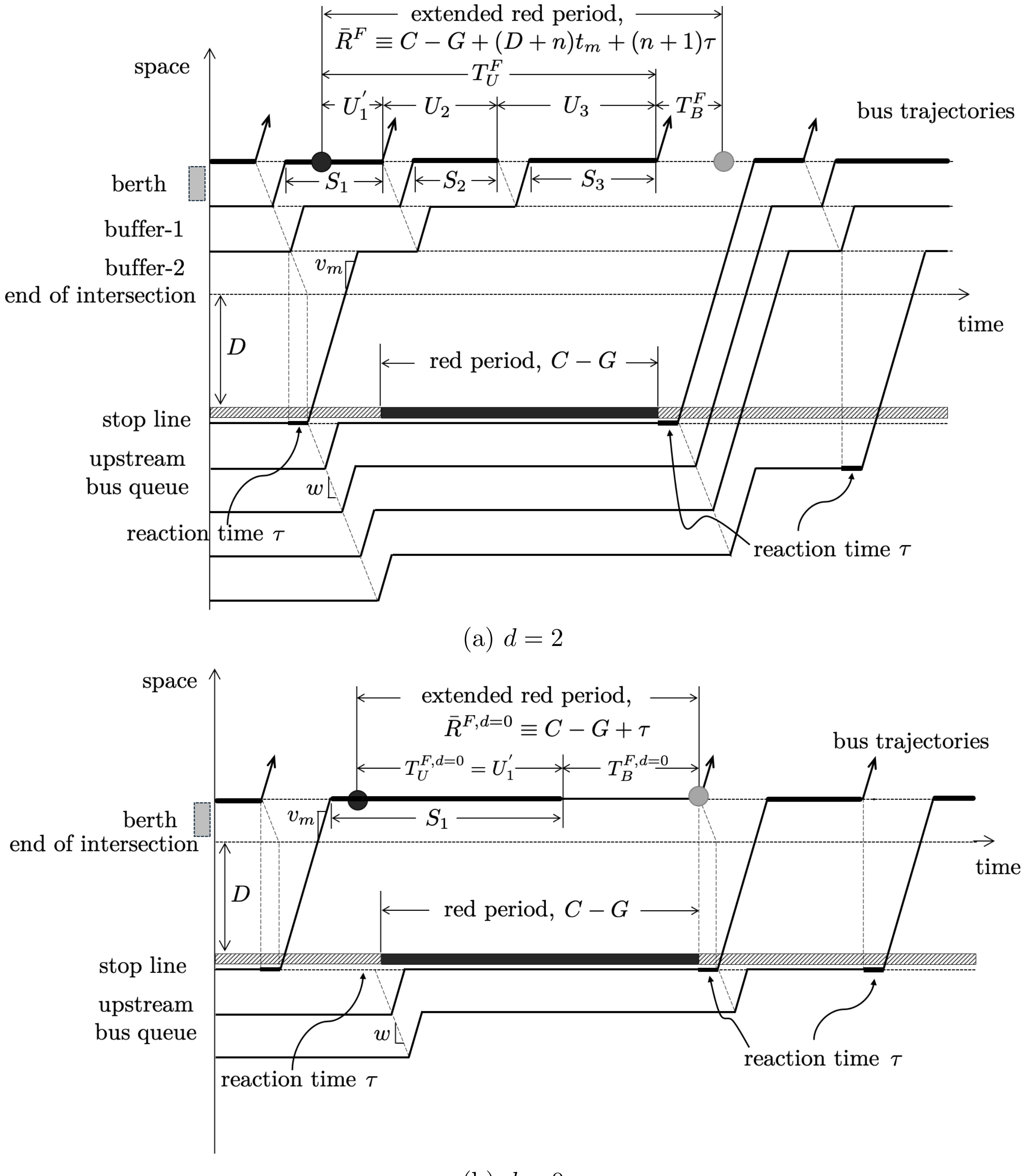


(a) $d = 2$

(b) $d = 0$

Figure 4: Time-space diagrams of bus operations at a single-berth far-side stop.

logic. First, a bus whose dwell time extends from the green period to beyond the black dot is the first bus trapped in the extended red period. Figure 4a reveals that whenever a bus finishes its service and departs the stop on or before the black dot, another bus queued upstream of the signal can always cross the intersection and fill up the buffer before the signal turns red. On the other hand, the first queued bus that can cross the intersection in the following green period will arrive at the berth no earlier than $\tau_m$ after the grey dot. If $(n+1)$ buses finish their services before the grey dot, the berth will be idle until the end of extended red period.

Hence, the duration of the extended red period for a single-berth far-side stop is $\bar{R}^F \equiv (n+1)\tau + C - G + (D+n)t_m$, where the superscript $F$ denotes the far-side stop case. Note that this is $Dt_m$ longer than the extended red period for a single-berth near-side stop, and the difference is exactly the time needed for a bus to travel through the intersection.

Now we denote the period during which the berth is vacant as $T_B^F$, which can be calculated by:

$$T_B^F = \max\{\bar{R}^F - T_U^F, 0\}, \tag{13}$$

where $T_U^F = U_1' + \sum_{j=2}^{n+1} U_j$ denotes the sum of dwell times, reaction times and move-up times of $n+1$ consecutive buses served in the extended red period; $U_1'$ and $U_j (j = 2, 3, ..., n+1)$ are defined in similar ways as for near-side stops. The $T_U^F$ is again approximated by a normal random variable with mean and variance given by equation (8). Consequently, the approximation of a single-berth far-side stop's capacity is calculated by (7) in which $r = \frac{\bar{R}-\mu_T}{\sigma_T}$ is replaced by $r = \frac{\bar{R}^F-\mu_T}{\sigma_T}$.

A special case arises when $d = n = 0$ (i.e., when the stop is placed immediately downstream of the intersection); see Figure 4b. In this case, a queued bus can discharge into the intersection only after seeing the berth becomes empty. Hence, the time gap between two consecutive buses' dwelling activities at the berth is now $\tau_m + Dt_m$ instead of $\tau_m$ in the case of $d > 0$. As a result, the duration of extended red period in this special case becomes $\bar{R}^{F,d=0} \equiv C - G + \tau$, because the first bus that crosses the intersection in the following green period should arrive at the berth no earlier than $\tau_m + Dt_m$ after the end of extended red period; see Figure 4b for the illustration. Under this special case, the approximate capacity is:

$$Q_{SA}^{F,d=0} = \frac{1}{1+\tau_m+Dt_m}\left(1 - \frac{\sigma_T^{F,d=0}\left(r^{F,d=0}\Phi(r^{F,d=0}) + \phi(r^{F,d=0})\right)}{C}\right), \tag{14}$$

where $r^{F,d=0} = \frac{\bar{R}^{F,d=0}-\mu_T^{F,d=0}}{\sigma_T^{F,d=0}}$ and

$$\begin{cases} \mu_T^{F,d=0} \approx \dfrac{C_S^2 + (1+\tau_m+Dt_m)^2}{2(1+\tau_m+Dt_m)}; \\ \left(\sigma_T^{F,d=0}\right)^2 \approx \dfrac{5+8(\tau_m+Dt_m)}{12(1+\tau_m+Dt_m)^2}C_S^4 + \dfrac{1}{2}C_S^2 + \dfrac{(1+\tau_m+Dt_m)^2}{12}. \end{cases} \tag{15}$$

The increased time gap $\tau_m + Dt_m$ would render the single-berth far-side stop with $d = 0$ a very bad design, as we shall see in Section 4.2.

### 2.2.2 Capacity approximation for a multi-berth far-side stop ($c \geq 2$ and $d = nc+d_0$)

Again, we first define the extended red period. As illustrated in Figure 5 for a 2-berth, 3-buffer far-side stop, the extended red period is again defined at the location of the upstream-most berth (berth-2 in the figure). A black dot is marked on the timeline of that location at $\delta_1^L \equiv (d+1)\tau + (c-1)\tau_m$ earlier than the red start. If a $c$-bus convoy completes service by the black dot, another $c$-bus convoy will discharge through the intersection to fill up the buffer before the present green period ends (which is the case shown in the figure). On the other hand, if the $c$-bus convoy completes service after $\delta_2^L \equiv (d+1)\tau$ ahead of the red start (not shown in the figure), then no additional bus is able to fill up the vacant space in the buffer before the green end. When the $c$-bus convoy completes service after $\delta_1^L$, but before $\delta_2^L$ ahead of the red start, a *small* convoy of less than $c$ buses will proceed to fill part of the vacancies in buffer. To simplify the modeling work, however, we ignore the possibility of having small convoys and define the extended red period's start time from an expectation perspective, i.e., at $\delta^L \equiv \frac{1}{2}(\delta_1^L + \delta_2^L) = (d+1)\tau + \frac{1}{2}(c-1)\tau_m$ before the red start.

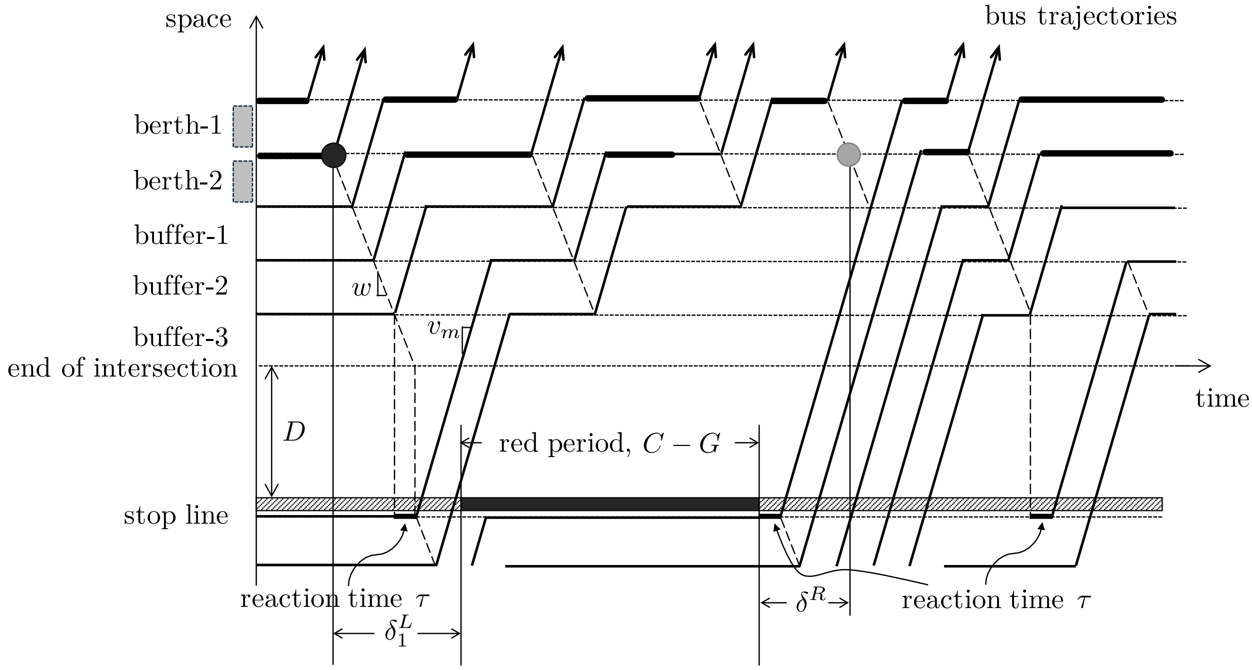


Figure 5: Time-space diagram of bus operations at a 2-berth, 3-buffer far-side stop.

The gray dot in Figure 5, which is located $\delta^R \equiv (D+d)t_m$ after the following green start, marks the end of extended red period. This is because the gray dot is $\tau_m$ ahead of the earliest time that a bus from the upstream queue can arrive at the upstream-most berth in the following green period. Hence, the length of extended red period is $\bar{R}^{Fp} \equiv C-G+\delta^L+\delta^R = C-G+(d+\frac{c+1}{2})\tau + (D+d+\frac{c-1}{2})t_m$.

We denote $T_U^F$ as the total time for serving all the convoys but the last smaller one (if any) in the extended red period; $T_P^F$ as the time for serving that last small convoy, during which the service rate is discounted by $\frac{c-d_0}{c}$ (if this small convoy does not exist, $T_P^F = 0$); and $T_B^F$ as the time when all the berths are vacant. These three variables are illustrated in Figure 6 for a 2-berth, 3-buffer far-side stop. For simplicity, we define the effective service time of full-size convoys as $T_U^{F'} \equiv T_U^F + \frac{d_0}{c}T_P^F$ and the effective idle time as $T_B^{F'} \equiv max\{\bar{R}^{Fp} - T_U^{F'}, 0\}$. The $T_U^{F'}$ can be expressed by:

$$T_U^{F'} = U_1^{p'} + \sum_{j=2}^{n+1} U_j^p + \frac{d_0}{c}U^{p,d_0}. \tag{16}$$

Similar to the near-side stop case, the mean $E[U^p]$ and variance $Var(U^p)$ of $U_j^p$ are given by (9). The $E[U_1^{p'}]$ and $Var(U_1^{p'})$ can be found in (D.6) of Appendix D as functions of $E[U^p]$ and $Var(U^p)$. When $d_0 \neq 0$, the $E[U^{p,d_0}]$ and $Var(U^{p,d_0})$ are obtained by substituting $d_0$ for

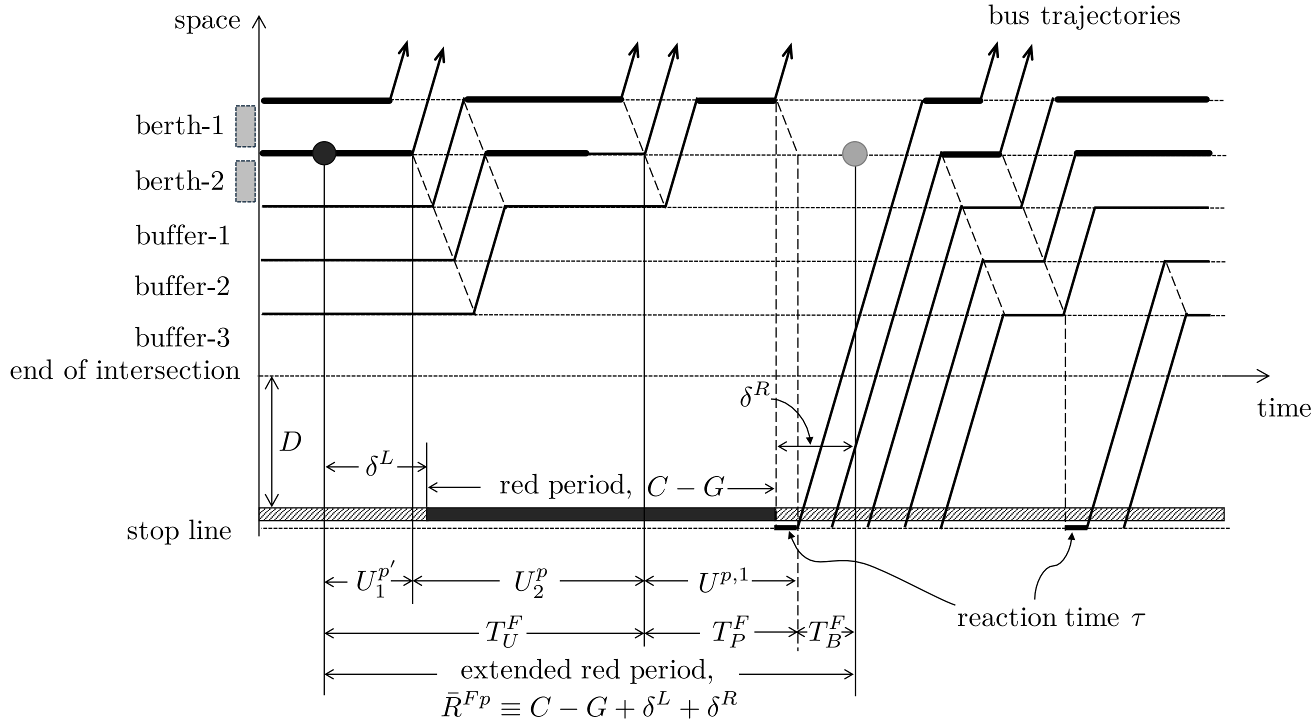


Figure 6: Time-space diagram of bus operations at a 2-berth, 3-buffer far-side stop where all the buffered buses are served within the extended red period.

some $c$ in (9):

$$\begin{cases} E[U^{p,d_0}] \approx 0.7931 C_S \log(d_0) + 0.9911 + c\tau_m; \\ Var(U^{p,d_0}) \approx 0.6819 C_S^3 \arctan(d_0) + 0.5102 C_S^2. \end{cases} \tag{17}$$

Hence, $\mu_{T_U^{F'}}$ and $\sigma^2_{T_U^{F'}}$ can be determined as follows:

$$\begin{cases} \mu_{T_U^{F'}} \approx E[U_1^{p'}] + nE[U^p] + \dfrac{d_0}{c} E[U^{p,d_0}]; \\ \sigma^2_{T_U^{F'}} \approx Var(T_1^{p'}) + nVar(U^{p'}) + \left(\dfrac{d_0}{c}\right)^2 Var(U^{p,d_0}). \end{cases} \tag{18}$$

The approximation of a multi-berth far-side stop's capacity is calculated by (11) where $\sigma_{T_U^{F'}}$ substitutes for $\sigma_{T_U'}$ and $r = \frac{\bar{R}^{Fp} - \mu_{T_U^{F'}}}{\sigma_{T_U^{F'}}}$. Note that this approximation only applies for the case of $d \geq 1$.

For the special case of $d = 0$, the time gap between two consecutive convoys becomes $c\tau_m + Dt_m$, and the extended red period becomes $\bar{R}^{Fp,d=0} \equiv C - G + (\frac{c+1}{2})\tau + (\frac{c-1}{2})t_m$. Thus the approximate capacity becomes:

$$Q_{MA}^{F,d=0} = \left(1 - \frac{\sigma_{T_U'}^{F,d=0}(r_p^{F,d=0}\Phi(r_p^{F,d=0}) + \phi(r_p^{F,d=0}))}{C}\right)\left(\frac{c}{h(c, C_S) + Dt_m}\right), \tag{19}$$

where $r_p^{F,d=0} = \frac{\bar{R}^{Fp,d=0} - \mu_{T_U'}^{F,d=0}}{\sigma_{T_U'}^{F,d=0}}$ and

$$\begin{cases} \mu_{T_U'}^{F,d=0} \approx \dfrac{(h(c,C_S)+Dt_m)^2 + Var(U^p)}{2(h(c,C_S)+Dt_m)}; \\ \left(\sigma_{T_U'}^{F,d=0}\right)^2 \approx \dfrac{(5h(c,C_S)+8Dt_m+3\tau_m)q^2(c,C_S)}{12(h(c,C_S)+Dt_m)^2(h(c,C_S)-c\tau_m)} + \dfrac{q(c,C_S)}{2} + \dfrac{(h(c,C_S)+Dt_m)^2}{12}. \end{cases} \tag{20}$$

The $q(c, C_S)$ and $h(c, C_S)$ are given by (9).

# 3 Model validation via simulation

In this section, we use computer simulation to examine the accuracy of the proposed approximations for near- and far-side stops. We develop event-based simulation programs for near- and far-side stops under the assumption that a bus queue is always present upstream of both the stop and the intersection. The pseudocode is furnished in Appendix E, and the detailed program code can be downloaded from: https://github.com/Minyu-Shen/Simulation-for-bus-stops-near-signalized-intersection. We also develop a program to visualize bus motions in the simulation. This program is used to validate the simulation. The visualization code is also provided in the above web link.

The parameter values used in the simulation are listed in Table 1. Stops with less-varied

Table 1: Parameter values for simulation validation and numerical analysis.

| Category | Parameter | Physical value | Normalized value |
|---|---|---|---|
| Bus stop design | $c$ | 1∼4 | – |
| | $d$ | 0∼4 | – |
| Bus operations | $\mu_S$ | 25 s | 1 |
| | $C_S$ | 0.3∼1 | – |
| Bus traffic characteristics | $s_j$ | 12 m | 1 |
| | $w$ | 25 km/h | 14.47 |
| | $v_m$ | 20 km/h | 11.57 |
| Signalized intersection | $C$ | 80∼240 s | 3.2∼9.6 |
| | $D$ | 24∼48 m | 2∼4 |
| | $G/C$ | 0.3∼0.7 | – |

dwell times, i.e., those with $C_S \in [0, 0.3)$, are not examined here since they are rare in reality. For each instance with specific values for $C_S$, $c$, $d$, $C$, $G/C$ and $D$, 300,000 buses are simulated to ensure that the average bus discharge rate converges to the steady-state capacity. To facilitate the readers' understanding of the numerical cases discussed in the following sections, the normalized capacity values obtained from our models were converted back to the actual physical values in the unit of "buses per hour".

Select validation results of the approximations are furnished in Section 3.1. Section 3.2 compares the simulated and approximate capacities against the TCQSM capacity formula (1).

## 3.1 Validation of the approximations

We first plot the approximate capacity and the simulated capacity against $C$ as dashed and solid curves, respectively, in Figures 7a-d. The four figures illustrate the results for four near-side stops with $c \in \{1, 2\}$ and $C_S \in \{0.3, 0.8\}$, respectively. We assume $G/C = 0.5$ in all the figures, and examine three values of $d$ in each figure: $d = 0, 2$, and 4. Stops with 3 or more berths exhibit similar results, which are omitted here in the interest of brevity.

Comparison between approximation and simulation results unveils that the approximation is quite accurate for most of the cases illustrated by the figures. The error is almost negligible for single-berth stops, and is consistently small for various values of $C$ and $d$. It grows as $c$ increases since great error is brought by the various approximation steps used in the multi-berth model (see Section 2.1.2). Moreover, for 2-berth near-side stops with large $C_S$ (Figure 7d), the approximation consistently underestimates the capacity. This is partly due to the overestimation of the intermediate variable $M$ in Appendix D. Finally, the error is larger for 2-berth stops with small $C_S$ (Figure 7c), because the approximation model fails to capture the high sensitivity of capacity to $C$ when $C_S$ is small. A brief explanation of this large error is that when $C_S$ is small, the service time of the first trapped convoy (or bus) is highly correlated with the signal timing (see the end of Section 2.1.1 and Appendix B). A more detailed explanation of the high sensitivity of capacity to $C$ is furnished below by using an extreme example of a 2-berth near-side stop with no buffer ($d = 0$), $G/C = 0.5$, and deterministic dwell time ($C_S = 0$). This stop's simulated capacity is plotted as the solid curve in Figure 8.

Note the first declining segment on the solid capacity curve for $80\,\text{s} \leq C < 134.6\,\text{s}$. For any $C$ in this range, only 4 buses are served per cycle (one 2-bus convoy in the red period and another convoy in the green). This is because $G = \frac{C}{2} < 67.3\,\text{s} = (\tau + 2\tau_m) + \mu_S + 2\tau_m + \mu_S$. The validity of the above inequality can be verified using the following parameter values: $\tau = s_j/w = 1.73\,\text{s}$, $t_m = s_j/v_m = 2.16\,\text{s}$, $\tau_m = \tau + t_m = 3.89\,\text{s}$, and $\mu_S = 25\,\text{s}$ (see Table 1). The reader can also verify by drawing a simple time-space diagram that $(\tau + 2\tau_m) + \mu_S + 2\tau_m + \mu_S$ is the minimum time needed for a 5th bus to discharge in a green period. Thus, as $C > 134.6\,\text{s}$, the stop capacity jumps to a higher value. (i.e., now 5 buses are served per cycle; see the small solid declining segment for $134.6\,\text{s} \leq C \leq 142.4\,\text{s}$ in Figure 8.) The 6th bus (which is in the same convoy as the 5th bus when entering the berths) will still be blocked by the red signal until $C > 142.4\,\text{s}$ (i.e., $G = \frac{C}{2} > 71.2\,\text{s} = (\tau + 2\tau_m) + \mu_S + 2\tau_m + \mu_S + \tau_m$). Hence we observe another capacity jump at $C = 142.4\,\text{s}$, beyond which 6 buses will be served per cycle. Consequently, the capacity curve exhibits a "sawtooth" shape, which is an intuitive result since when the bus dwell time is deterministic, the number of buses that can be served in a green period "jumps" as the green duration exceeds certain thresholds.

The "sawteeth" in the curve would be gradually smoothed as $C_S$ increases, as illustrated by the dotted, dashed, and dash-dot curves in Figure 8, which represent the cases of $C_S = 0.1$, 0.2, and 0.3, respectively. The fluctuations also diminish as $C$ or $d$ increases, because a larger $C$ (and thus a larger $G$ when $G/C$ is fixed) means more buses will be served in each green period, and a larger $d$ means more buses can potentially be served in each red period. In both cases, the "capacity jumps" created by serving one additional bus per cycle will be diluted. We also see by comparing Figures 7a and c that the capacity fluctuations are larger for a large $c$. This is because a larger convoy size $c$ will render the convoy dwell time $U^p$ (see equation (C.1) in Appendix C) less varied; i.e., the coefficient of variation $\frac{\sqrt{Var(U^p)}}{E[U^p]}$ will decrease with $c$.

Finally, the above capacity fluctuations are not captured by our models, which rely on the CLT approximation. Hence the approximations would be inaccurate when $C_S$ is very small. Fortunately, this issue is of lesser practical concern since in the real world $C_S$ is usually no less than 0.4 (St. Jacques and Levinson, 1997; Levinson and St. Jacques, 1998; Bian et al., 2015).

The accuracy of our approximation is further examined by box plots of the percentage approximation error, $|\frac{Q_{\text{appx}}-Q_{\text{sim}}}{Q_{\text{sim}}}|$, where $Q_{\text{appx}}$ is the approximate capacity and $Q_{\text{sim}}$ is the simulation result. These box plots are shown in Figures 9a-c for near-side stops with $c = 1, 2, 3$, respectively; each figure displays the results for $C_S \in \{0.3, 0.55, 0.8\}$ and $d \in \{0, 1, 2, 3, 4\}$. Each error box represents the distribution of the percentage errors for a set of $C$ values ranging from 80 s to 240 s and a fixed $G/C = 0.5$. Specifically, each box spans the range from the first quartile to the third quartile of the error distribution; the band inside each box indicates the median; and the whiskers above and below each box indicate the maximum and minimum errors (save for the outliers if any), respectively.

First note that most errors are less than 1% for single-berth stops (Figure 9a), 3% for 2-berth stops (Figure 9b), and 5% for 3-berth stops (Figure 9c). The errors increase with $c$ because: i) the multi-berth model incorporates more approximation steps than the single-berth model; and ii) for a fixed $d$ and $C$, a larger $c$ means fewer convoys will be served in an extended red period, which will render the CLT approximation less accurate.

For a given $c$, the largest error always occurs with the smallest $C_S$ and $d = 0$ (see the outliers on top of the left-most box plot in each figure). This is mainly due to the uncaptured high sensitivity of capacity to $C$ when $C_S$ is small (see the explanation above).

It is also observed in Figures 9b and c that for a fixed $C_S$ and $c$, the error generally diminishes with $d$. The reason is simple: a larger $d$ means more convoys can potentially be served in an extended red period, thus rendering a more accurate CLT approximation. This effect is not observed in Figure 9a since for single-berth stops the error is already very small regardless of the value of $d$, and other factors may be dominating as $d$ grows. Nevertheless, in all the cases examined here, the CLT approximation is quite good even when $d = 0$, which is a little surprising to us. This maybe partly due to the bell-shaped distributions used for bus dwell times, which are similar to the shape of normal PDFs.

Similar findings are obtained when comparing the approximation against simulation results for far-side stops; see Figures 7e and f for a 2-berth far-side stop with $D = 3$ and $C_S = 0.3$ and 0.8, respectively, and Figures 10a-c for box plots of approximation errors for far-side stops with $D = 3$, $C_S \in \{0.3, 0.55, 0.8\}$, $d \in \{0, 1, 2, 3, 4\}$, and $c = 1, 2, 3$, respectively. Comparisons between Figures 7c and e and between Figures 9a-c and Figures 10a-c unveil that the far-side stop models have larger errors when $C_S$ is small, due to the greater sensitivity of far-side stop capacity to $C$. When $C_S$ is large and $c = 2$ and 3, however, the far-side stop models exhibit

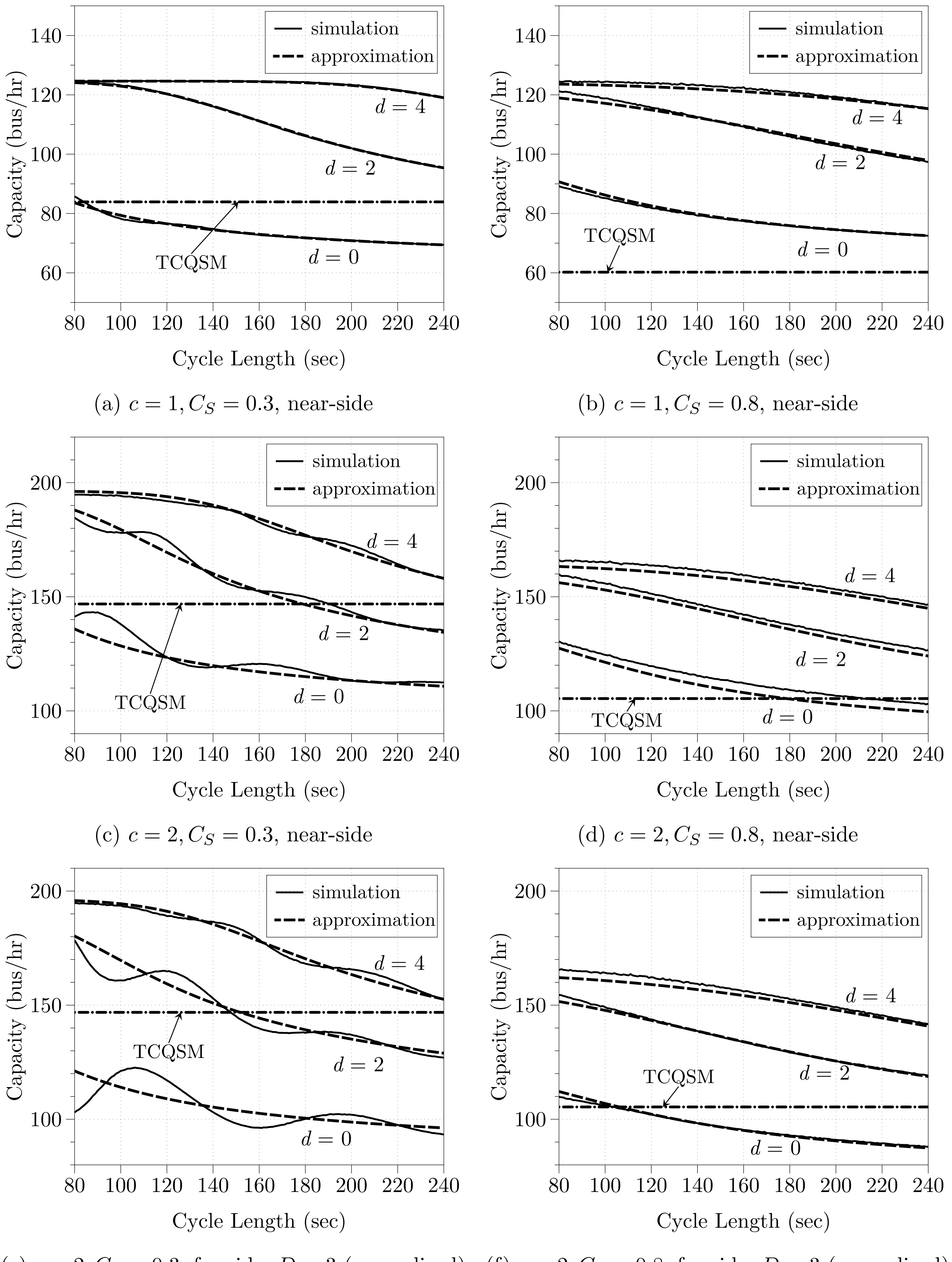


(a) $c = 1, C_S = 0.3$, near-side (b) $c = 1, C_S = 0.8$, near-side

(c) $c = 2, C_S = 0.3$, near-side (d) $c = 2, C_S = 0.8$, near-side

(e) $c = 2, C_S = 0.3$, far-side, $D = 3$ (normalized) (f) $c = 2, C_S = 0.8$, far-side, $D = 3$ (normalized)

Figure 7: Validation of the approximations.

smaller errors than the near-side ones. This is mainly due to the larger error that occurs when estimating $M$ in the multi-berth near-side stop model (see Appendix D).

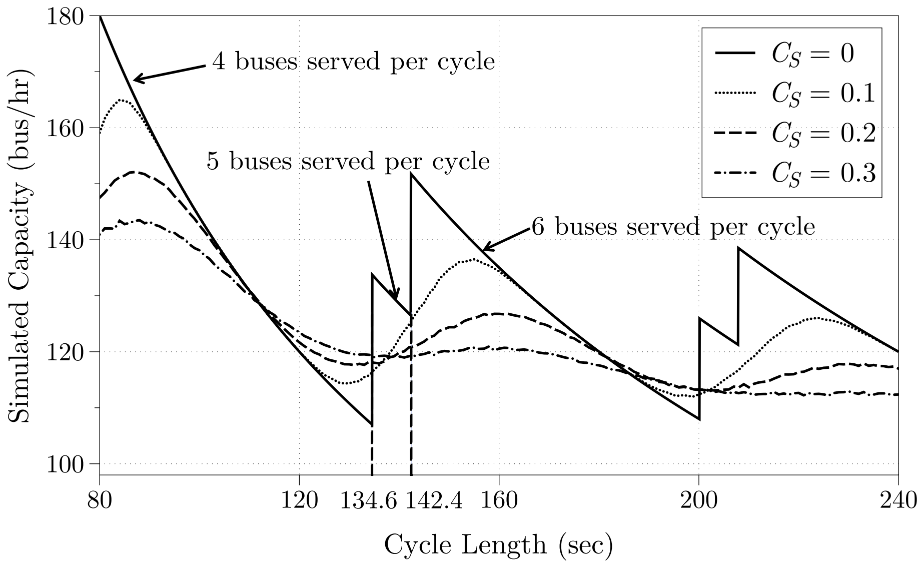


Figure 8: Sensitivity of capacity to $C$ when $C_S \leq 0.3$ ($c = 2$, $d = 0$, near-side stop).

Though only the results for $c = 1 \sim 3$ are shown here, our approximation also performs fairly good for $c = 4$, where the errors in most cases are far below 10%. For $c = 5$ and 6, however, errors between 10% and 20% appear more frequently, mainly because the convoy dwell time $U^p$ has a very small coefficient of variation.

## 3.2 Comparison against the TCQSM capacity formula

We now use the same simulation results to validate the TCQSM formula (1), and compare its accuracy with our approximation. The capacity calculated from (1) is plotted as the dash-dot line in each of Figures 7a-f. The parameters in (1) take the following values: the effective berth number $N_{el}$ is set to 1 and 1.75 for single and double-berth stops, respectively, according to Exhibit 6-63 in TCQSM (Kittelson & Associates, Inc., 2013); $f_{tb} = 1$ since we assume the bus operations are not affected by other traffic; the clearance time $t_c$ is equal to $\tau_m$ since the re-entry delay is zero for bus stops located in dedicated lanes; the operating margin coefficient, $Z$, is set to 0.675 since TCQSM claims that this value would yield the maximum capacity of the stop; the mean dwell time $t_d = \mu_S$; and the coefficient of variation in dwell time $c_v = C_S$. The TCQSM formula is independent of the buffer size $d$ and the cycle length $C$ (given a fixed green ratio $G/C$). Hence, only one horizontal line is plotted in each of Figures 7a-f.

Comparison between the dash-dot curve and the solid curves unveils how far the TCQSM estimate is from the ground truth. Note first how the simulated capacity varies with $C$ and $d$, and that these effects are totally ignored by the TCQSM formula. Even for the case of $d = 0$ (under which it is believed that the TCQSM formula is developed), the TCQSM formula's error is above 10% for most cases, and can be up to 50% (see Figure 7c). This is because the operating margin term in (1), $Zc_vt_d$, is too sensitive to $c_v$. Closer examination of the solid curves in these figures unveils that the ratio between the capacities of a 2-berth stop and a single-berth stop (given other parameter values are equal), i.e., the "effective number of berths" for a 2-berth curbside stop, is not a constant. In fact this ratio varies with all the relevant parameters examined here: $C$, $d$ and $C_S$. Finally, the TCQSM formula treats the near- and far-side stops in the same way, while in reality a near-side stop produces a higher capacity than its far-side

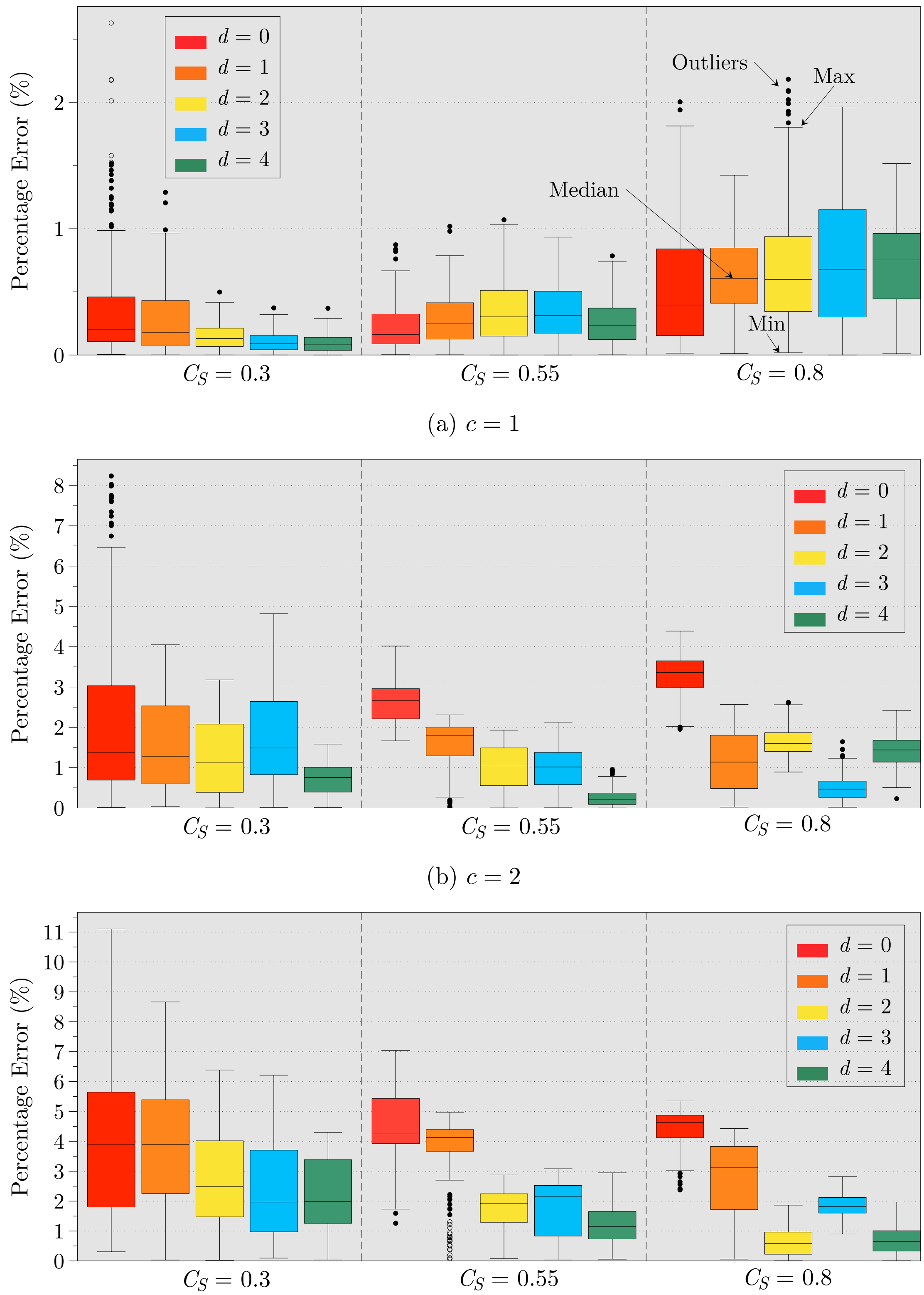


(a) $c = 1$

(b) $c = 2$

(c) $c = 3$

Figure 9: Box plots of percentage error between approximations and simulation results for near-side bus stops.

counterpart. (The reason of this and more comparisons between near- and far-side stops are furnished in Section 4.2.)

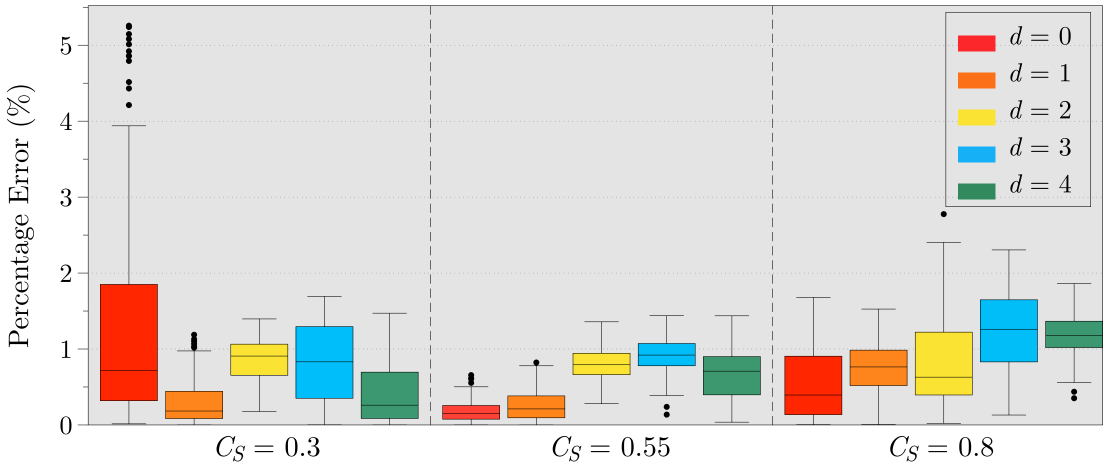


(a) $c = 1$

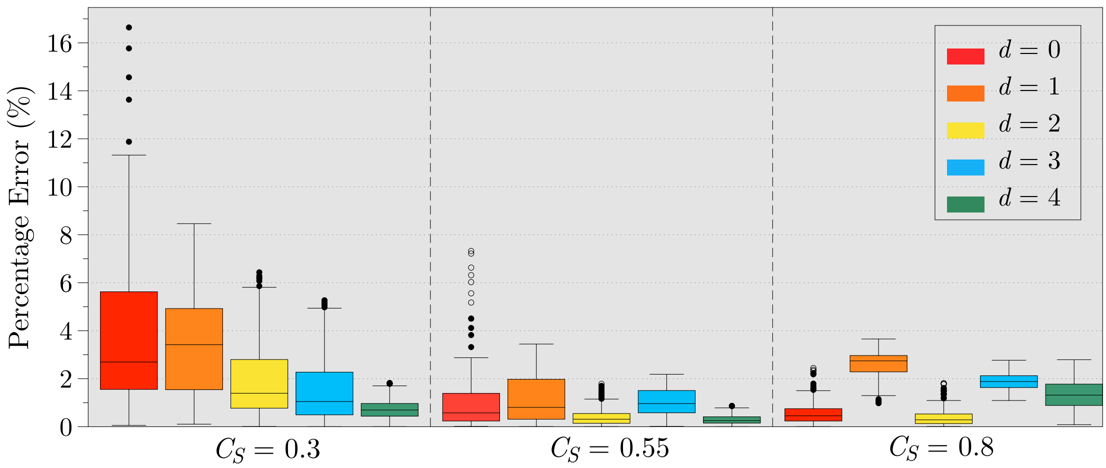


(b) $c = 2$

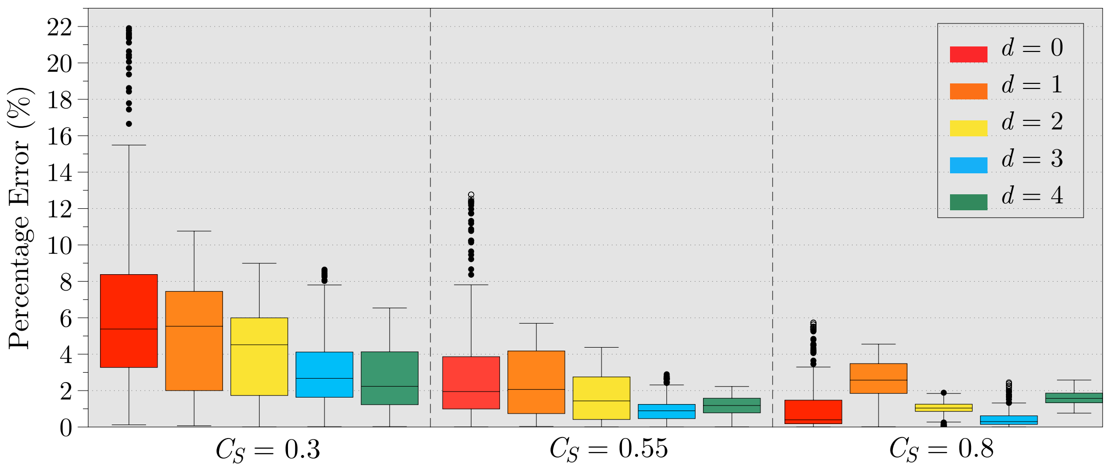


(c) $c = 3$

Figure 10: Box plots of percentage error between approximations and simulation results for far-side bus stops.

# 4 Numerical analysis

We now examine broader ranges of numerical instances using the approximation models, i.e., equations (7), (11), (14) and (19), and discuss their practical implications. Section 4.1 examines the discounting effect of the neighboring signal on the stop's capacity, and how this effect depends on various operating factors, especially the buffer size $d$. Section 4.2 discusses which side of the intersection to better place a stop at, when the objective is to improve the bus-carrying capacity. We still use the parameter values in Table 1 in the following sections.

## 4.1 Capacity discounting effect of the signal

From equations (2) and (10), we see that the percentage capacity loss caused by the signal can be simply expressed by $\frac{E[T_B]}{C}$ for a single-berth stop and $\frac{E[T_B^{'}]}{C}$ for a multi-berth stop. Figures 11a and b plot this percentage capacity loss against the red period duration for instances with $C_S = 0.4$ and 0.8, respectively. Each figure contains 12 curves representing 12 scenarios with $c \in \{1, 2, 3\}$ and $d \in \{0, 1, 2, 3\}$. We use different line types to mark curves with different $c$: solid for $c = 1$, dotted for $c = 2$, and dashed for $c = 3$; and different colors to mark curves with different $d$: black for $d = 0$, red for $d = 1$, blue for $d = 2$, and green for $d = 3$. We choose red period duration as the horizontal axis because the numerators of percentage capacity loss, $E[T_B]$ and $E[T_B^{'}]$, are functions of red period duration only, and are independent of $C$. The scaling effect of $C$ on the percentage capacity loss can thus be isolated from other factors, and be simply illustrated by using different vertical axes, one for each value of $C$. (Three vertical axes for $C = 100\,$s, $130\,$s and $160\,$s, respectively, are used in the figures.)

In each figure, comparing the curves of the same line type unveils that the capacity loss drops rapidly as $d$ grows. For example, note how the capacity loss drops from 55% to 3% when $d$ increases from 0 to 3 for a single-berth stop with $C = 100\,$s and a red period of $70\,$s, as marked by the four black dots in Figure 11a. For a larger $c$, the capacity loss drops with the increase of $d$ at a slower speed. This is intuitive because more buffer spaces are needed to mitigate the signal's negative impacts on the capacity of a large stop. Similar results are also observed for far-side stops, which are omitted here in the interest of brevity.

The above results can be used to determine how far from the intersection a stop should be placed to achieve a certain percentage, $\theta$, of an isolated stop's capacity. This is useful in practice because transit agencies often prefer to place a stop in the proximity of the intersection to facilitate passengers' access and transfers, and to reduce the number of unprotected street crossings (Fitzpatrick et al., 1996). The buffer size $d$ required to achieve a target percentage $\theta$ is a function of $c$, $C_S$, $C$, and $G/C$, which can be calculated numerically from (7) and (14) for single-berth stops, and (11) and (19) for multi-berth stops. Some tabulated values of the critical $d$ for near-side stops when $\theta = 95\%$ are furnished in Appendix F.

The effect of $c$ on the capacity loss is a little more complicated. When $d = 0$, the capacity loss decreases as $c$ grows. This is because only one convoy is served in an extended red period, and a larger convoy will increase the utilization of the red period. On the other hand, the

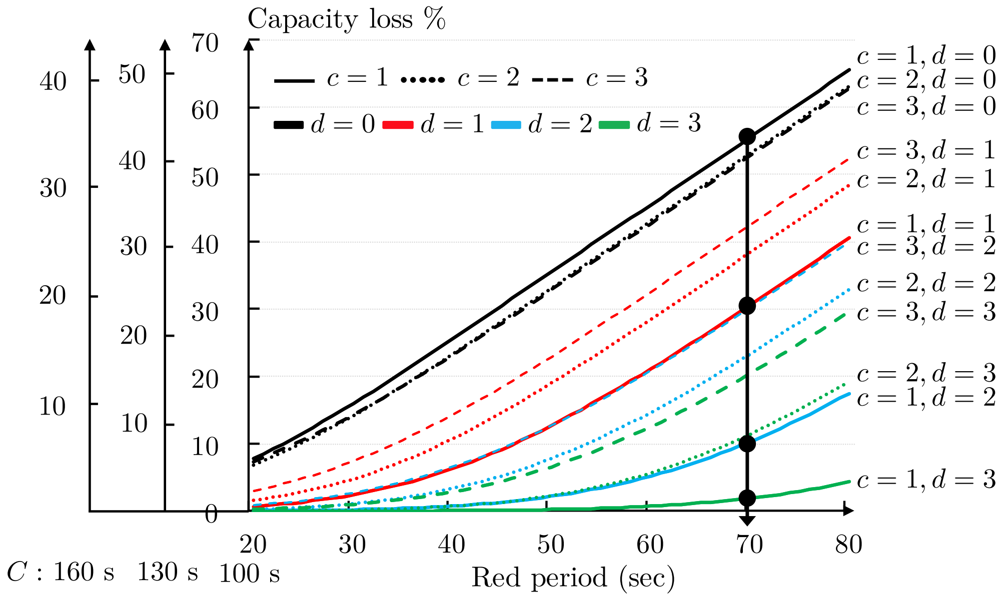


(a) $C_S = 0.4$

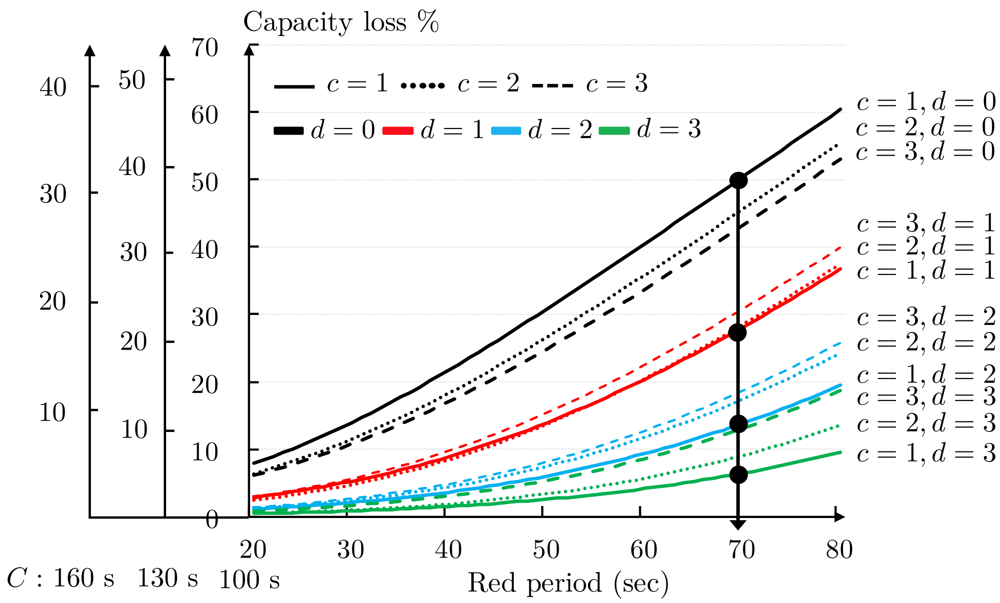


(b) $C_S = 0.8$

Figure 11: Percentage capacity loss resulting from the signal for near-side stops.

capacity loss increases with $c$ for any $d > 0$, since in this case the number of convoys that can be served in an extended red period drops as $c$ grows. Lastly, comparison between Figures 11a and b unveils that for multi-berth stops, the damage done by the signal is smaller for a larger $C_S$. This is because a larger $C_S$ renders a longer convoy service time, and thus more of an extended red period will be utilized for serving the convoys. However, this is not true for single-berth stops.

## 4.2 Comparison between near- and far-side stops

There has been a long debate on which side of the intersection is better for the placement of a bus stop (Terry and Thomas, 1971; Fitzpatrick et al., 1996). Factors that may affect this decision include safety reasons, potential conflicts between dwelling buses and turning traffic, passenger accessibility, etc. (Fitzpatrick et al., 1996). There exist a number of studies that quantified and compared the benefits and costs of near- and far-side stops. But most of them have significant limitations because they relied on simulation of specific stop layouts or empirical data collected from specific sites (Zhao et al., 2007; Li et al., 2012; Diab and El-Geneidy, 2015; Cvitanić, 2017). On the other hand, computationally efficient analytical models that can be used to examine the general cases are rare. The latter kind of models include Furth and SanClemente (2006) and Gu et al. (2014). However, these two works focused on comparing the bus and car delays at near- and far-side stops where at most one bus would arrive in each signal cycle. Thus they said nothing about busy bus stops where bus queues are often present.

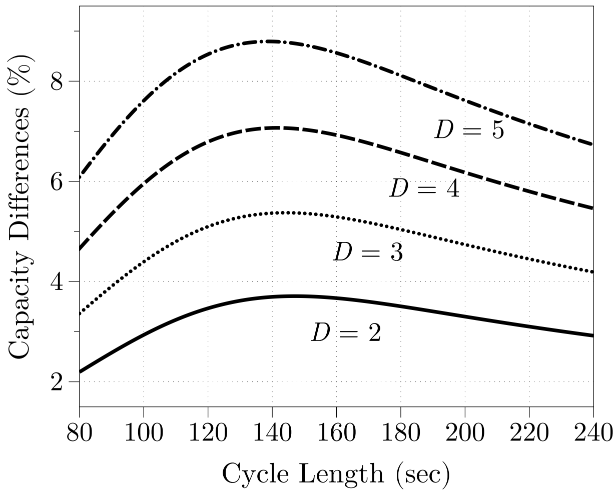


(a) $c = 2, d = 2$

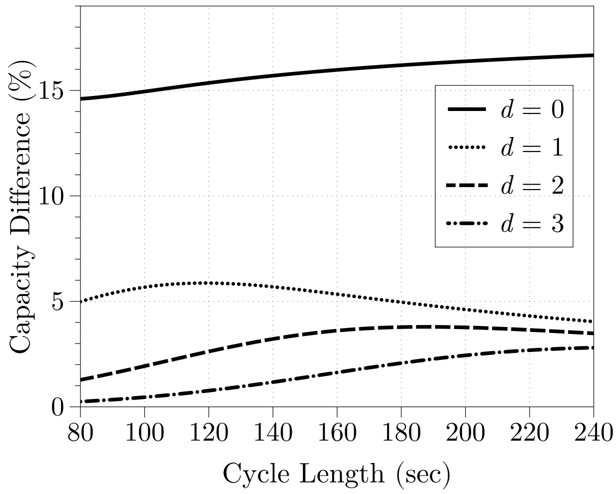


(b) $c = 1, D = 3$

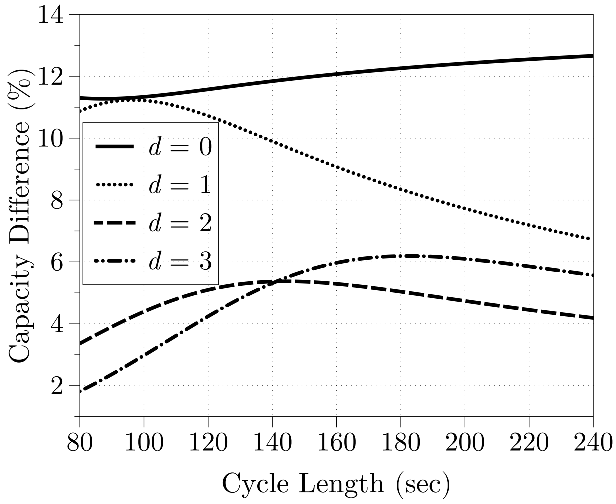


(c) $c = 2, D = 3$

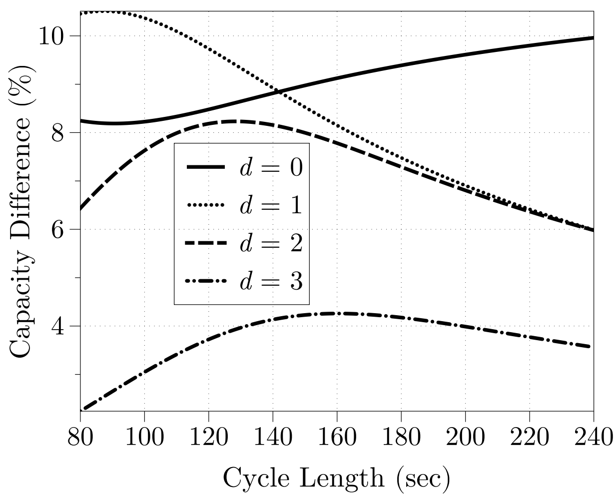


(d) $c = 3, D = 3$

Figure 12: Capacity comparison between near- and far-side stops with $G/C = 0.5$ and $C_S = 0.5$.

Using our approximation models, we plot in Figure 12a the percentage of difference in capacity between near- and far-side stops, $\frac{Q_{\text{ns}}-Q_{\text{fs}}}{Q_{\text{ns}}}$, where $Q_{\text{ns}}$ and $Q_{\text{fs}}$ denote the capacities of near-side and far-side stops, respectively. Four curves are plotted in the figure for $D = 2, 3, 4, 5$ (normalized), respectively, and for $c = 2$, $d = 2$, $G/C = 0.5$ and $C_S = 0.5$. All the four curves are above 0, which indicates that a near-side stop always produces a higher bus-carrying capacity than its far-side counterpart, should other conditions be the same. This is mainly because a far-side stop's extended red period is longer than that of a near-side stop due to the extra term of $Dt_m$; see the equations of $\bar{R}$ in Section 2.1.1, $\bar{R}^p$ in Section 2.1.2, $\bar{R}^F$ in Section 2.2.1, and $\bar{R}^{Fp}$ in Section 2.2.2. The term $Dt_m$ is added because at a far-side stop buses queued upstream have to travel across the intersection to reach the stop. This also explains why the capacity difference diminishes as $D$ decreases, as shown in the figure. Hence, a bus stop should be placed at the near side of an intersection, if the bus-carrying capacity is the major concern. Interestingly, this is on the contrary to the finding in Gu et al. (2014), which states that far-side stops are more favorable since they produce less bus delay than near-side ones. Note again that the above-cited work applies only to stops with low to medium bus traffic.

We further plot the percentage capacity differences against $C$ for $c = 1, 2, 3$ in Figures 12b-d, respectively, where $D$ is assumed to be 3. Each figure contains four curves representing the cases of $d = 0, 1, 2, 3$, respectively. The figures show that the advantage of near-side stops by-and-large diminishes as $d$ increases. This is also intuitive because when $d$ is sufficiently large, the capacities of near- and far-side stops both approach that of an isolated stop. Figure 12b also shows that a single-berth far-side stop is particularly unproductive when $d = 0$ (over 15% capacity difference for $d = 0$ versus less than 6% for $d = 1$). This can also be explained using our models: note in this case that the time gap between two consecutive buses increases from $\tau_m$ to $\tau_m + Dt_m$ (see Section 2.2.1). In Figures 12c and d, however, the gap between the capacity differences for $d = 0$ and $d = 1$ becomes smaller. This is because, for far-side stops with $c > 1$, a convoy will discharge through the intersection together, which dilutes the negative effect of the extra term $Dt_m$.

# 5 Conclusions

We develop analytical approximations for single- and multi-berth curbside stops located in dedicated bus lanes and near signalized intersections. Our approximations have closed-form formulas, except for the standard normal CDF (i.e. $\Phi(r)$), which itself has several good closed-form approximations in the literature (e.g. Vazquez-Leal et al., 2012). Our models are more accurate and general than the methods in previous studies and professional handbooks, because they explicitly account for the effects of key operating factors that were overlooked in the literature (e.g., the signal cycle length and the buffer size) and the characteristics of bus traffic (e.g., the move-up time and reaction time). Extensive simulation tests manifest that in most cases the approximation error is within 5%. Larger approximation errors may arise when $C_S$ is small, $c$ is large, and $d$ is small.

Our accurate and computationally-efficient approximations can be conveniently used by practitioners to replace the flawed capacity formulas of curbside bus stops in the professional handbooks. They can be used, e.g., to determine the appropriate design and location of a new bus stop for serving a predicted peak-hour bus flow, or to assess the performance of measures for mitigating bus congestion at an existing stop. Measures to be considered would include adding berths and increasing the distance between stop and intersection (recall that our models can furnish critical distances needed to reduce or eliminate the capacity discounting effect of neighboring signals; see again Appendix F). Strategies that can reduce the mean and variance of bus dwell times (e.g., using wider bus doors, low-floor buses, and off-board fare collection) can also be assessed by our models for near- and far-side stops. In addition, practitioners may also consider to decrease the signal cycle length while keeping the green ratio unchanged. This would reduce the red period duration and thus significantly increase a near- or far-side stop's capacity (see again Figures 7 and 11) without affecting the general-purpose (GP) traffic's discharging capacity at the intersection by much. (Note that this measure would be deemed to have no effect if the TCQSM formula (1) is used.) Finally, a congested far-side stop can be relocated to the near-side of intersection to gain up to 15% of additional capacity (see again Figures 12a-d), although this capacity gain diminishes as $d$ increases.

Admittedly, many numerical results presented in this paper can also be generated through simulation. Still, our analytical approach is useful due to the following reasons:

1. Some general insights can be immediately inferred from the capacity formulas or from our analytical derivation, but would be difficult to obtain directly from simulation. For example, equations (2) and (10) show that the percentage capacity loss due to the signal ($\frac{E[T_B]}{C}$ or $\frac{E[T_B']}{C}$) is inversely proportional to cycle length; and the formulas for $E[T_B]$ and $E[T_B']$ (e.g. equation (6)) reveal that this percentage capacity loss is a non-linear function of red period duration. Hence the effect of signal on bus-stop capacity is not as simple as described in the TCQSM formula (1). Built upon these insights, we further conclude that stop capacity can be increased by reducing red period duration (or cycle length) while keeping the green ratio unchanged. These insights also inspire us to create diagrams similar to Figures 11a and b, where the effects of cycle length and red period duration are clearly illustrated for stops with various sizes and locations. Note how these diagrams can be used by practitioners in the design of near- and far-side stops.

   As another example, note how the formulas of extended red periods reveal the significant differences between capacities of near-side and far-side stops, given that other conditions are equal. Capacity formulas for far-side stops with no buffer ($d = 0$) further unveil why this is a very bad design in terms of stop capacity. Note that it would be difficult to reveal and confirm these general findings using simulation results, since there are numerous scenarios to simulate under various operating parameters.

2. The analytical approach can help us better understand the cause-and-effect relationships behind the key factors affecting bus-stop capacity. Many findings from the numerical

results can thus be explained; please refer to Section 4 for details. Understanding of these findings is very useful for practitioners to make appropriate design decisions under diverse operating environments. On the other hand, simulations are “black boxes” that usually cannot furnish straightforward explanations of those causal relations.

3. Parsimonious analytical models are always desirable for their convenience in practical use. This is why simple formulas or procedures described in professional handbooks (e.g. TCQSM and HCM) are still embraced by practitioners despite their well-known flaws, and despite the fact that commercial simulation tools become more and more powerful today. In addition, simulation is often much more time-consuming than applying analytical formulas (even if the latter may require some numerical computation, like in our case). In practice, an accurate analytical model can be used in the initial stage of a design project to identify a few promising options, and the more detailed and realistic simulation can be employed to select from those few design options and fine-tune the final design.

To be sure, our approximations are limited in that they apply only to scenarios where: i) an exclusive bus lane is present; ii) the green period is long enough to discharge all the queued buses for a near-side stop, or to fill up the vacant buffer and berths of a far-side stop; and iii) bus overtaking maneuvers are prohibited. Potential extensions of the present work to address some of the above limitations are discussed as follows.

In reality, buses discharging from a near-side stop may compete against right-turning GP traffic for the buffer space. For this case, the distribution of buffer spaces occupied by right-turning vehicles can be approximated using right-turning vehicles’ arrival process and the bus discharge rate into the buffer. This distribution can then be incorporated into our stop capacity approximation to account for the impact of right-turning traffic. A similar approach can be used to account for the impact of (through-moving) GP vehicle queues on the capacity of a near-side bus bay stop, where exiting buses have to merge back to the GP traffic lanes. For far-side bus bay stops without bus lane, exiting buses may be blocked when they are waiting for a sufficient gap in the GP traffic to merge back. This effect can be estimated by incorporating a stochastic merge model into the approximation.

For a near-side stop, if the green period is too short to discharge $c+d$ queued buses, residual bus queues may exist in the buffer at the end of some green periods. This case is difficult to model since bus operations in neighboring cycles are highly correlated. One potential approach is to model the residual queue lengths by a Markov chain, but closed-form approximations of stop capacity would not be available. Fortunately, such a case is rare in reality (see Footnote 3). On the other hand, a far-side stop with a short green period is equivalent to a far-side stop with a smaller buffer, for which our present approximations can be directly applied.

# Acknowledgements

The research was supported by an Early Career Scheme (Project No. 25200614) provided by the Research Grants Council of Hong Kong and a start-up grant provided by the Hong Kong Polytechnic University.

# Appendix A List of notations

Table A.1: List of notations

| Notation | Description |
|---|---|
| **Input parameters** | |
| $c$ | Number of berths |
| $C$ | Cycle length |
| $C_S$ | Coefficient of variation in bus dwell time |
| $d$ | Number of buffer spaces |
| $D$ | Length of signalized intersection |
| $G$ | Green period duration |
| $n, d_0$ | Parameters satisfying $d = nc + d_0$ when $n = 0, 1, 2, ...$, and $0 \leq d_0 < c$ |
| $s_j$ | Jam spacing / berth length |
| $t_m$ | Time for a bus to travel forward through one berth |
| $\tau$ | Reaction time of a bus |
| $\mu_S$ | Mean of bus dwell time |
| $v_m$ | Bus's move-up speed |
| $w$ | Backward wave speed of bus traffic |
| **Other parameters and variables** | |
| $\delta^L, \delta^R$ | Start and end time of extended red period, respectively, for a multi-berth far-side stop |
| $M$ | Number of buses in a multi-berth near-side stop at the start of an extended red period |
| $\bar{R}, \bar{R}^F$ | Extended red periods for single-berth near- and far-side stops, respectively |
| $\bar{R}^p, \bar{R}^{Fp}$ | Extended red periods for multi-berth near- and far-side stops, respectively |
| $\bar{R}^{F,d=0}, \bar{R}^{Fp,d=0}$ | Extended red periods for single- and multi-berth far-side stops with $d = 0$, respectively |
| $T_B, T_B^F$ | Times during which the stop is fully blocked for near-side stops or vacant for far-side stops, respectively |
| $T_B^{'}, T_B^{F'}$ | Effective blockage time for a near-side stop and effective vacant time for a far-side stop, respectively |
| $T_P, T_P^F$ | Times of serving the last small convoy (if any) for multi-berth near- and far-side stops, respectively |
| $T_U, T_U^F$ | Total times for serving $n+1$ consecutive buses in an extended red period for single-berth near- and far-side stops, respectively; and total times for serving all the full-size convoys in an extended red period for multi-berth near- and far-side stops, respectively. |
| $T_U^{'}, T_U^{F'}$ | Effective service time of full-size convoys for near- and far-side stops, respectively |
| $U_1^{'}, U_1^{p'}$ | Portions of times for serving the first trapped bus (for single-berth stops) and convoy (for multi-berth stops) in the extended red period, respectively |
| $U_j$ | Sum of dwell time, reaction time and move-up time of $j$-th bus. |
| $U_j^p$ | Total time for serving the $j$-th convoy |
| $U^{p,x}$ | Time for serving the last small convoy of size $x$ in the extended red period |
| $\mu_T, \sigma_T^2$ | Mean and variance of $T_U$, respectively |
| $\mu_{T_U^{'}}, \sigma^2_{T_U^{'}}$ | Mean and variance of $T_U^{'}$, respectively |
| $\mu_{T_U^{F'}}, \sigma^2_{T_U^{F'}}$ | Mean and variance of $T_U^{F'}$, respectively |

# Appendix B Derivation of approximations (8)

First, we have $E[U_j] = 1 + \tau_m$ and $Var(U_j) = Var(S_j) = C_S^2$. Due to the mutual independence between $U_1'$ and $U_j$'s, $\mu_T$ and $\sigma_T^2$ can be obtained as follows:

$$\begin{cases} \mu_T = n(1+\tau_m) + E[U_1']; \\ \sigma_T^2 = nC_S^2 + Var(U_1'). \end{cases} \tag{B.1}$$

The $E[U_1']$ and $Var(U_1')$ are derived by assuming that the start of the extended red period is a *random incidence* within a renewal process of consecutive bus departures from the stop. By the definition of random incidence (Larson and Odoni, 1981), the renewal interval that contains the random incidence, $W$, has the following PDF:

$$f_W(t) = \frac{tf_U(t)}{E[U]} = \frac{tf_S(t-\tau_m)}{1+\tau_m}, \tau_m \leq t \leq \infty, \tag{B.2}$$

where $f_U$ is the PDF of $U_j = S_j + \tau_m (j = 1, 2, ..., n+1)$, and $f_S$ is the PDF of $S_j$.

Conditioning on $W$, $U_1'$ is uniformly distributed in $[0, W]$. Thus, we have:

$$\begin{aligned} E[U_1'] &= E\left[E[U_1' \mid W]\right] = E\left[\frac{1}{2}W\right] = \frac{1}{2}\int_{\tau_m}^{\infty} t \cdot \frac{tf_S(t-\tau_m)}{1+\tau_m}dt \\ &= \frac{1}{2(1+\tau_m)}\int_0^{\infty}(u+\tau_m)^2 \cdot f_S(u)du = \frac{E[S^2] + 2\tau_m + \tau_m^2}{2(1+\tau_m)}. \end{aligned}$$

$$\begin{aligned} Var(U_1') &= E\left[U_1'^2\right] - (E[U_1'])^2 = E\left[E[U_1'^2 \mid W]\right] - (E[U_1'])^2 = E\left[\frac{1}{3}W^2\right] - (E[U_1'])^2 \\ &= \frac{1}{3(1+\tau_m)}\int_0^{\infty}(u+\tau_m)^3 \cdot f_S(u)du - (E[U_1'])^2 \\ &= \frac{E[S^3] + 3\tau_m E[S^2] + 3\tau_m^2 + \tau_m^3}{3(1+\tau_m)} - (E[U_1'])^2. \end{aligned}$$

Since $S_j$ follows a gamma distribution with mean 1, by using its moment generating function, we can calculate that $E[S^2] = C_S^2 + 1$ and $E[S^3] = 2C_S^4 + 3C_S^2 + 1$. Thus, we have:

$$E[U_1'] = \frac{C_S^2 + (\tau_m + 1)^2}{2(1+\tau_m)}; \tag{B.3}$$

$$Var(U_1') = \frac{5+8\tau_m}{12(1+\tau_m)^2}C_S^4 + \frac{1}{2}C_S^2 + \frac{(1+\tau_m)^2}{12}. \tag{B.4}$$

Plugging (B.3) and (B.4) into (B.1), we have:

$$\begin{cases} \mu_T \approx n(1+\tau_m) + \dfrac{C_S^2 + (1+\tau_m)^2}{2(1+\tau_m)}; \\ \sigma_T^2 \approx \dfrac{5+8\tau_m}{12(1+\tau_m)^2}C_S^4 + (\dfrac{1}{2} + n)C_S^2 + \dfrac{(1+\tau_m)^2}{12}. \end{cases} \tag{8}$$

The above approximations rely on the hypothetical uncorrelation between $U_1'$ and signal timing. Their performance would be poor if $C_S$ is small. For example, in the deterministic case where $C_S = 0, \tau_m = 0$ and $C - \bar{R} = 2.99$, we have $U_1' = 0.01$, while (B.3) gives $E[U_1'] = 0.5$. But if $C - \bar{R}$ increases slightly from 2.99 to 3.01, we would have $U_1' = 0.99$ while (B.3) still gives $E[U_1'] = 0.5$. Hence the distribution of $U_1'$ and the stop capacity can be highly sensitive to signal timing when $C_S$ is small. Note that if $C_S > 0$, the correlation between $U_1'$ and signal phases diminishes as green duration increases, and so does the sensitivity of stop capacity to signal timing.

# Appendix C Derivation of approximation (9)

Figure C.1 shows the bus trajectories of a 3-bus convoy dwelling at a 3-berth stop. From the figure, we have:

$$U^p = max\{S_1, S_2, ..., S_c\} + c\tau_m, \tag{C.1}$$

where $S_j(j = 1, 2, ..., c)$ denotes the dwell time of the $j$-th bus in the convoy.

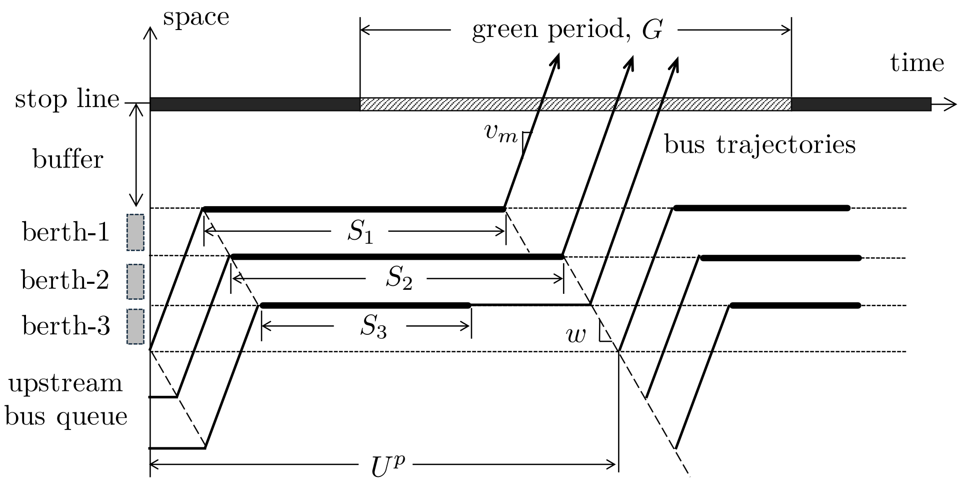


Figure C.1: Time-space diagram of bus operations at a 3-berth near-side stop.

From (C.1), we can obtain the CDF of $U^p$ as follows:

$$F_{U^p}(t) = (F_S(t - c\tau_m))^c \quad \text{for} \quad t \geq c\tau_m, \tag{C.2}$$

where $F_S$ is the CDF of $S_j$. Since $S_j$ is a non-negative continuous random variable, we have:

$$E[U^p] = c\tau_m + \int_0^\infty (1 - (F_S(t))^c)\, dt. \tag{C.3}$$

Similarly,

$$Var(U^p) = 2\int_0^\infty t\,(1 - (F_S(t))^c)\, dt - \left(\int_0^\infty (1 - (F_S(t))^c)\, dt\right)^2. \tag{C.4}$$

The two integrals in equations (C.3) and (C.4) are the first and second raw moments of the order statistic $max\{S_1, S_2, ..., S_c\}$; see David and Nagaraja (2004) for the detailed derivations. Unfortunately, there is neither closed-form expressions nor good approximations for these moments, save for a few very special cases (David and Nagaraja, 2004). In light of this, we here fit least squares models to tabulated values of these moments when $S_j$ follows a gamma distribution with $C_S \in [0.2, 1]$ and $1 \le c \le 6$. (Note that the above parameter ranges have covered most of the curbside stops in the real world; for example, Levinson and St. Jacques (1998) concluded from empirical data that $C_S \in [0.4, 0.8]$, and stops containing more than 6 berths are also rare in the real world.) The tabulated values were furnished by Gupta (1960) and Prescott (1974). Our best-fitted models selected from numerous candidates with various mathematical forms are:

$$\begin{cases} E[U^p] \approx h(c, C_S) \equiv 0.7931 C_S \log(c) + 0.9911 + c\tau_m; \\ Var(U^p) \approx q(c, C_S) \equiv 0.6819 C_S^3 \arctan(c) + 0.5102 C_S^2. \end{cases} \tag{9}$$

The goodness-of-fit of (9) is illustrated in Figure C.2a for $E[U^p]$ and Figure C.2b for $Var(U^p)$ for the realistic ranges of $c$ and $C_S$, where the dashed curves represent the fitted models and the solid curves represent the tabulated values furnished by the literature. The root-mean-square error (RMSE) of the above models are 0.0125 and 0.0131, respectively; and the R-squared values are 0.9984 and 0.9992, respectively.

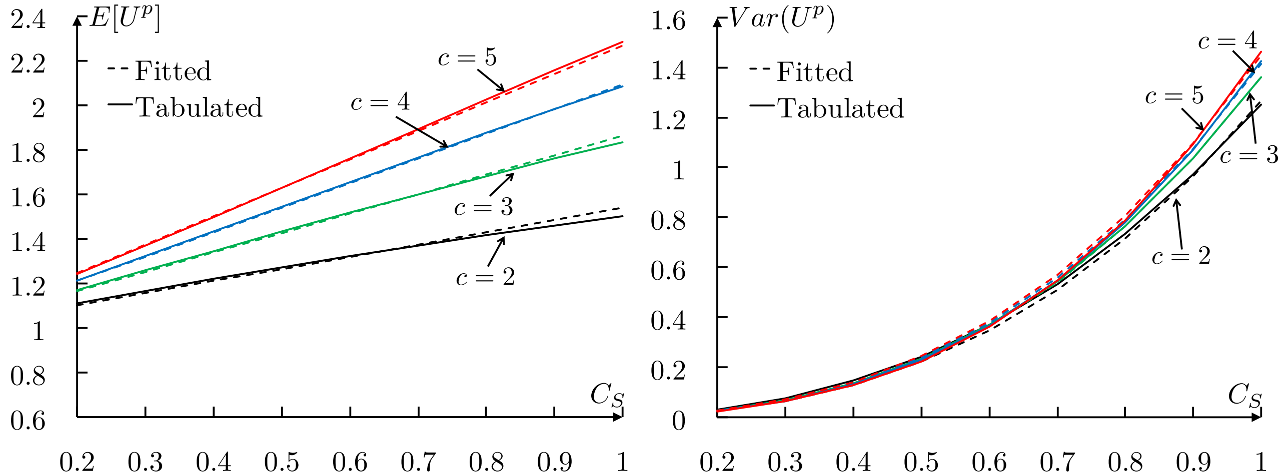


(a) $E[U^p]$ (b) $Var(U^p)$

Figure C.2: Goodness-of-fit for (9).

# Appendix D Derivation of approximations (12)

The $T_U'$ depends on $T_U$, $N_P$, and $T_P$, which all depend upon the number of buses in the stop at the start of the extended red period. We denote this number as $M$ ($1 \le M \le c$). (Note that some of these $M$ buses may have completed their services, but they are blocked by buses residing in the downstream berths.) Depending on the value of $M$, the following three cases may arise:

1. If $M < d_0$, $(n+1)$ full-size convoys can be served following the first convoy in the extended red period. The $(n+3)$-th convoy would be a small one with only $d_0 - M$ buses. Thus we have:

$$\begin{cases} T_U = U_1^{p'} + \sum_{j=2}^{n+2} U_j^p; \\ N_P = d_0 - M; \\ T_P = U^{p,d_0-M}, \end{cases} \tag{D.1}$$

where $U_1^{p'}$ denotes the portion of the first convoy's service time that is contained in the extended red period; $U_j^p$ $(j = 2, 3, ..., n+2)$ the time for serving the $j$-th (full-size) convoy; and $U^{p,d_0-M}$ the time for serving the small convoy of $d_0 - M$ buses.

2. If $M = d_0$, we have:

$$\begin{cases} T_U = U_1^{p'} + \sum_{j=2}^{n+2} U_j^p; \\ N_P = 0; \\ T_P = 0. \end{cases} \tag{D.2}$$

3. If $d_0 < M \leq c$, only $n$ full-size convoys can be served following the first one, and the $(n+2)$-th convoy would be a small one with $c + d_0 - M$ buses. Thus,

$$\begin{cases} T_U = U_1^{p'} + \sum_{j=2}^{n+1} U_j^p; \\ N_P = c + d_0 - M; \\ T_P = U^{p,c+d_0-M}. \end{cases} \tag{D.3}$$

The $E[T_U']$ and $Var(T_U')$ can be derived given the distribution of $M$, which depends upon $c$ and the bus dwell time distribution. Unfortunately, the distribution of $M$ is very difficult to derive analytically, even for special (e.g. gamma) distributions of bus dwell times. Hence we again seek an approximation to solve this issue.

We find by extensive numerical experiments for bus stops with $c \leq 6$ that, if the start of the extended red period is treated as a random incidence in the first convoy's service time (similar to the assumption made in Appendix B for single-berth stops), and if the bus dwell times follow a gamma distribution with $C_S \in [0.1, 1]$, then $M \geq c - 1 \geq d_0$ for 85.8% of the time. This is also intuitive: while some buses of the convoy may have completed their services earlier, they may not be able to depart the stop as long as there is one bus still dwelling at a downstream berth. We henceforth ignore the above case 1 and consider cases 2 and 3 only. Cases 2 and 3 can be further combined into one case described by the following equation:

$$T_U^{'} \approx U_1^{p'} + \sum_{j=2}^{n+1} U_j^p + \frac{c+d_0-M}{c} U^{p,c+d_0-M}. \tag{D.4}$$

We further use the following approximations:

$$\begin{cases} \mu_{T_U^{'}} \equiv E[T_U^{'}] \approx E[U_1^{p'}] + nE[U^p] + E[\frac{c+d_0-M}{c} U^{p,c+d_0-M}] \\ \qquad \approx E[U_1^{p'}] + nE[U^p] + \frac{c+d_0-E[M]}{c} E[U^{p,c+d_0-E[M]}]; \\ \sigma^2_{T_U^{'}} \equiv Var(T_U^{'}) \approx Var(U_1^{p'}) + nVar(U^p) + Var(\frac{c+d_0-M}{c} U^{p,c+d_0-M}) \\ \qquad \approx Var(U_1^{p'}) + nVar(U^p) + \left(\frac{c+d_0-E[M]}{c}\right)^2 Var(U^{p,c+d_0-E[M]}). \end{cases} \tag{D.5}$$

The mean and variance of $U_1^{p'}$ are obtained by the following approximations in which the start of the extended red period is treated as a random incidence:

$$\begin{cases} E[U_1^{p'}] \approx \frac{E^2[U^p] + Var(U^p)}{2E[U^p]}; \\ Var(U_1^{p'}) \approx \frac{5E[U^p] + 3\tau_m}{12E^2[U^p](E[U^p] - c\tau_m)} Var^2(U^p) + \frac{Var(U^p)}{2} + \frac{E^2[U^p]}{12}. \end{cases} \tag{D.6}$$

Section D.1 presents the derivation of (D.6).

We also have $E[U^{p,c+d_0-E[M]}] \approx h(c+d_0-E[M], C_S)$ and $Var(U^{p,c+d_0-E[M]}) \approx q(c+d_0-E[M], C_S)$; see equations (9). Finally, the value of $E[M]$ is again approximated by a fitted least-square model as follows (with RMSE = 0.061 and $R^2 = 0.9974$):

$$E[M] \approx 0.9617c - 0.1899 \cdot c \cdot C_S. \tag{D.7}$$

Plugging (9), (D.6) and (D.7) into (D.5) and simplifying, we have (12).

## D.1 Derivation of (D.6)

We again use the random incidence assumption adopted in Appendix B. In addition, we approximate $S^p \equiv \max\{S_1, S_2, ..., S_c\}$ as a gamma-distributed random variable with the same mean $E[S^p]$ and variance $Var(S^p)$. Using the moment generating function of gamma distribution, we find that $E[S^{p2}] = E^2[S^p] + Var(S^p)$ and $E[S^{p3}] = E^3[S^p] + 3E[S^p]Var(S^p) + \frac{2Var^2(S^p)}{E[S^p]}$. The renewal interval that contains the random incidence, $W$, has the following PDF:

$$f_W(t) = \frac{tf_{U^p}(t)}{E[U^p]} = \frac{tf_{S^p}(t-c\tau_m)}{E[S^p]+c\tau_m}, c\tau_m \le t \le \infty. \tag{D.8}$$

Conditioning on $W$, $U_1^{p'}$ is uniformly distributed in $[0, W]$. So,

$$E[U_1^{p'}] = E\left[\frac{1}{2}W\right] = \frac{1}{2(E[S^p] + c\tau_m)} \int_0^{\infty} (u + c\tau_m)^2 \cdot f_{S^p}(u)du$$
$$= \frac{(E[S^p] + c\tau_m)^2 + Var(S^p)}{2(E[S^p] + c\tau_m)} = \frac{E[U^p]}{2} + \frac{Var(U^p)}{2E[U^p]}. \quad \text{(D.9)}$$

$$Var(U_1^{p'}) = E\left[\frac{1}{3}W^2\right] - (E[U_1^{p'}])^2$$
$$= \frac{1}{3(E[S^p] + c\tau_m)} \int_0^{\infty} (u + c\tau_m)^3 \cdot f_S(u)du - (E[U_1^{p'}])^2$$
$$= \frac{E[S^{p3}] + 3c\tau_m E[S^{p2}] + 3(c\tau_m)^2 E[S^p] + (c\tau_m)^3)}{3(E[S^p] + c\tau_m)} - (E[U_1^{p'}])^2$$
$$= \frac{5E[U^p] + 3c\tau_m}{12E^2[U^p](E[U^p] - c\tau_m)} Var^2(U^p) + \frac{Var(U^p)}{2} + \frac{E^2[U^p]}{12}. \quad \text{(D.10)}$$

# Appendix E Simulation algorithms

The following notation is used in this simulation:

$B_i$ - The number of berth in which the $i$-th bus dwells, counting from the downstream-most berth, which is numbered berth 1;

$F_i$ - The number of buffer space at which the $i$-th bus waits, counting from the downstream-most buffer space, which is numbered buffer 1; $F_i = 0$ means that the bus is not in any buffer; $F_i > d$ means that the bus is blocked immediately after service;

$LQ_i$ - Time when the $i$-th bus leaves the upstream queue;

$ES_i$ - Time when the $i$-th bus finishes service;

$WB_i$ - The $i$-th bus's waiting time in the berth after service;

$LB_i$ - The $i$-th bus's departure time from the berth;

$WF_i$ - The $i$-th bus's waiting time in the buffer due to the red signal (for near-side stops only);

$FT_i$ - The number of moves that the $i$-th bus makes in the buffer area before entering a berth (for far-side stops only);

$LFN_i$ - The time when the $i$-th bus leaves the buffer and discharges into the intersection (for near-side stops only).

$LFF_{i,j}$ - The time when the $i$-th bus makes the $j$-th move in the buffer area (for far-side stops only; $j \in [1, 2, ..., FT_i]$).

**Algorithm 1:** Simulation of bus operations at a near-side bus stop.

- Generate the service times according to a given distribution with $\mu_S$ and $C_S$;
- Set states of the first bus: $LQ_1 \leftarrow 0$, $B_1 \leftarrow 1$, $ES_1 \leftarrow LQ_1 + ct_m + S_1$, $LB_1 \leftarrow ES_1$;
- **if** $mod(LB_1 + dt_m, C) \leq G$ **then**
  - $F_1 \leftarrow 0$, $WF_1 \leftarrow 0$;
- **else**
  - $F_1 \leftarrow 1$, $WF_1 \leftarrow C - mod(LB_1 + dt_m, C) + \tau$, $LFN_1 \leftarrow WF_1 + LB_1 + dt_m$;
- **foreach** *simulated bus* $i \geq 2$ **do**
  - **if** $B_{i-1} < c$ **then**
    - $LQ_i \leftarrow LQ_{i-1} + \tau_m$, $B_i \leftarrow B_{i-1} + 1$;
  - **else**
    - **if** $F_{i-1} < d + c$ **then**
      - **if** $F_{i-1} < d$ **then**
        - $B_i \leftarrow 1$;
      - **else**
        - $B_i \leftarrow F_{i-1} - d + 1$;
      - $LQ_i = LQ_{i-1} + (c - B_{i-1} + 1)t_m + S_{i-1} + WB_{i-1} + \tau$;
    - **else**
      - $B_i \leftarrow 1$, $LQ_i = LFN_{i-1} + \tau$;
  - $ES_i \leftarrow LQ_i + (c - B_i + 1)t_m + S_i$;
  - $WB_i \leftarrow max(0, LB_{i-1} + \tau - ES_i)$, $LB_i \leftarrow ES_i + WB_i$;
  - **if** $F_{i-1} = 0$ **or** $F_{i-1} = d + c$ **then**
    - **if** $RM_i \leftarrow mod(LB_i + (B_i + d - 1)t_m, C) \leq G$ **then**
      - $F_i \leftarrow 0$, $WF_i \leftarrow 0$, $LFN_i \leftarrow LB_i$;
    - **else**
      - $F_i \leftarrow 1$, $WF_i \leftarrow C - RM_i + \tau$, $LFN_i \leftarrow LB_i + (B_i + d - 1)t_m + WF_i$;
  - **else**
    - **if** $LFN_{i-1} + \tau \leq LB_i + (B_i + d - F_{i-1} - 1)t_m$ **then**
      - **if** $RM_i \leftarrow mod(LB_i + (B_i + d - 1)t_m, C) \leq G$ **then**
        - $F_i \leftarrow 0$, $WF_i \leftarrow 0$, $LFN_i \leftarrow LB_i$;
      - **else**
        - $F_i \leftarrow 1$, $WF_i \leftarrow C - RM_i + \tau$, $LFN_i \leftarrow LB_i + (B_i + d - 1)t_m + WF_i$;
    - **else**
      - $F_i \leftarrow F_{i-1} + 1$, $WF_i \leftarrow LFN_{i-1} + \tau - LB_i - (B_i + d - F_i)t_m$, $LFN_i = LFN_{i-1} + \tau$;

**Algorithm 2:** Simulation of bus operations at a far-side bus stop.

Generate the service times according to a given distribution with $\mu_S$ and $C_S$;
Set states of the first bus: $LQ_1 \leftarrow 0$, $F_1 \leftarrow 0$, $FT_1 \leftarrow 0$, $B_1 \leftarrow 1$,
$ES_1 \leftarrow LQ_1 + (c + d + D)t_m + S_1$, $WB_1 \leftarrow 0$, $LB_1 \leftarrow ES_1$;
**foreach** *simulated bus* $i \geq 2$ **do**
  **if** $F_{i-1} = 0$ **then**
    **if** $B_{i-1} = c$ **then**
      **if** $d = 0$ **then**
        $B_i \leftarrow 1$, $F_i \leftarrow 0$; **if** $temp \leftarrow mod(LB_{i-1} + \tau, C) \leq G$, **then**
        $LQ_i \leftarrow LB_{i-1} + \tau$, **else**, $LQ_i \leftarrow C - temp + LB_i + \tau$; **endif**
        $LB_i = ES_i \leftarrow LQ_i + (c + d + D)t_m + S_i$;
      **else**
        **if** $mod(LQ_{i-1} + \tau_m, C) \leq G$ **then**
          $LQ_i \leftarrow LQ_{i-1} + \tau_m$, $F_i = B_i = FT_i \leftarrow 1$, $LFF_{i,1} \leftarrow LB_{i-1} + \tau$,
          $LB_i = ES_i \leftarrow LFF_{i,1} + ct_m + S_i$;
        **else if** $temp \leftarrow C - mod(LQ_{i-1}, C) + LQ_{i-1} + \tau < LB_{i-1} + \tau$ **then**
          $F_i = B_i = FT_i \leftarrow 1$, $LFF_{i,1} \leftarrow LB_{i-1} + \tau$,
          $LB_i = ES_i \leftarrow LFF_{i,1} + ct_m + S_i$;
        **else**
          $LQ_i = temp$, $FT_i = F_i \leftarrow 0$, $B_i \leftarrow 1$,
          $LB_i = ES_i \leftarrow LQ_i + (c + d + D)t_m + S_i$;
    **else**
      $F_i \leftarrow 0$; **if** $mod(LQ_{i-1} + \tau_m, C) \leq G$ **then**
        $LQ_i \leftarrow LQ_{i-1} + \tau_m$, $B_i \leftarrow B_{i-1} + 1$,
        $ES_i \leftarrow LQ_i + (c + d - B_i + 1 + D)t_m + S_i$,
        $LB_i \leftarrow ES_i + max(0, LB_{i-1} + \tau - ES_i)$;
      **else if** $temp \leftarrow C - mod(LQ_{i-1} + \tau_m, C) + LQ_{i-1} + \tau_m + \tau < LB_{i-1} + \tau$ **then**
        $LQ_i \leftarrow LB_{i-1} + \tau$, $B_i \leftarrow B_{i-1} + 1$,
        $LB_i = ES_i \leftarrow LQ_i + (d + c - B_i + 1 + D)t_m + S_i$;
      **else**
        $LQ_i \leftarrow temp$, $B_i \leftarrow 1$, $LB_i = ES_i \leftarrow LQ_i + (c + d + D)t_m + S_i$;
  **else if** $F_{i-1} < d$ **then**
    **if** $mod(LQ_{i-1} + \tau_m, C) \leq G$ **then**
      $LQ_i \leftarrow LQ_{i-1} + \tau_m$, $F_i \leftarrow F_{i-1} + 1$, $B_i \leftarrow$ Berth($F_i$);
    **else**
      $LQ_i \leftarrow LQ_{i-1} + C - mod(LQ_{i-1}, C) + \tau$, Which-buffer-berth();
    When-leave-buffer-berth();
  **else**
    **if** $mod(LFF_{i-1,1} + \tau, C) \leq G$ **then**
      $LQ_i \leftarrow LFF_{i-1,1} + \tau$, Which-buffer-berth();
    **else**
      $LQ_i \leftarrow LFF_{i-1,1} + \tau + C - mod(LFF_{i-1,1} + \tau, C) + \tau$, Which-buffer-berth();
    When-leave-buffer-berth();

**Function** `Berth`($x$):
    **if** $mod(x, c) = 0$ **then**
        **return** $c$;
    **else**
        **return** $mod(x, c)$;

**Function** `Which-buffer-berth()`:
    $flag \leftarrow 0$;
    **for** $k = 1 : 1 : FT_{i-1}$ **do**
        **if** $LQ_i + (d - F_{i-1} + (k-1)c + 1 + D)t_m < LFF_{i-1,k} + \tau$ **then**
            **if** $F_{i-1} < d$ **then**
                $F_i = F_{i-1} - (k-1)c + 1$;
            **else**
                **if** $k = 1$, **then**, $F_i \leftarrow d - c + 1$, **else**, $F_i \leftarrow F_{i-1} - (k-1)c + 1$, **endif**;
            $B_i \leftarrow \mathrm{Berth}(F_i)$, $flag \leftarrow 1$, **break**;
    **if** $flag = 0$ **then**
        **if** $LQ_i + (d + c - B_{i-1} + D)t_m < LB_{i-1} + \tau$ **then**
            **if** $B_{i-1} = c$, **then**, $B_i = F_i \leftarrow 1$, **else**, $F_i \leftarrow 0$, $B_i \leftarrow B_{i-1} + 1$, **endif**;
        **else**
            $F_i \leftarrow 0$, $B_i \leftarrow 1$;

**Function** `When-leave-buffer-berth()`:
    $FT_i \leftarrow \mathrm{ceil}(F_i/c)$;
    **if** $FT_i = 0$ **then**
        $ES_i \leftarrow LQ_i + (c + d - B_i + 1 + D)t_m + S_i$,
        $LB_i \leftarrow max(0, LB_{i-1} + \tau - ES_i) + ES_i$;
    **else if** $FT_i = FT_{i-1}$ **then**
        **if** $(mod(F_i, c) = 1$ **and** $c \neq 1)$ **or** $c = 1$ **then**
            **For** $k = 1 : 1 : FT_i - 1$, **do** $LFF_{i,k} \leftarrow LFF_{i-1,k+1} + \tau$, **endfor**;
            $LFF_{i,FT_i} \leftarrow LB_{i-1} + \tau$;
        **else**
            **For** $k = 1 : 1 : FT_i$, **do** $LFF_{i,k} \leftarrow LFF_{i-1,k} + \tau$, **endfor**;
    **else if** $FT_i > FT_{i-1}$ **then**
        **For** $k = 1 : 1 : FT_{i-1}$, **do** $LFF_{i,k} \leftarrow LFF_{i-1,k} + \tau$,**endfor**;
        $LFF_{i,FT_i} \leftarrow LB_{i-1} + \tau$;
    **else**
        **if** $(mod(F_i, c) = 1$ **and** $c \neq 1)$ **or** $c = 1$ **then**
            $LFF_{i,FT_i} \leftarrow LB_{i-1} + \tau$;
            **For** $k = FT_{i-1} : -1 : 1$, **do** $LFF_{i,k} \leftarrow LFF_{i-1,FT_{i-1}-FT_{i+k}} + \tau$, **endfor**;
            $LFF_{i,FT_i} \leftarrow LB_{i-1} + \tau$;
        **else**
            **For** $k = FT_i : -1 : 1$, **do** $LFF_{i,k} \leftarrow LFF_{i-1,FT_{i-1}-FT_{i+k}} + \tau$, **endfor**;
    $ES_i \leftarrow LFF_{i,FT_i} + ct_m + S_i$, $LB_i \leftarrow max(0, LB_{i-1} + \tau - ES_i) + ES_i$;

# Appendix F Tables of critical $d$ to eliminate the negative effect of the signal on a near-side stop's capacity

Tables F.1a-d furnish the values of the critical $d$ for various $c$, $G/C$, $C_S$ and $C$ and $\theta = 95\%$. Note that the values of $C$ are normalized as multiples of $\mu_S$. The practitioners can use interpolation between neighboring tabulated values to calculate the critical $d$ if the relevant parameter values cannot be directly found in the tables.

Table F.1: Critical $d$ to ensure a near-side stop's capacity is no less than 95% of the capacity of a corresponding isolated stop.

(a) $c = 1$

| | | $C$ | | | | |
|---|---|---|---|---|---|---|
| $G/C$ | $C_S$ | 3 | 4 | 5 | 6 | 7 |
| 0.35 | 0.4 | 2 | 3 | 3 | 4 | 5 |
| | 0.6 | 2 | 3 | 4 | 4 | 5 |
| | 0.8 | 3 | 4 | 4 | 5 | 5 |
| 0.5 | 0.4 | 2 | 2 | 3 | 3 | 3 |
| | 0.6 | 2 | 2 | 3 | 3 | 4 |
| | 0.8 | 2 | 3 | 3 | 4 | 4 |
| 0.65 | 0.4 | 1 | 1 | 2 | 2 | 2 |
| | 0.6 | 1 | 2 | 2 | 2 | 2 |
| | 0.8 | 2 | 2 | 2 | 2 | 3 |

(b) $c = 2$

| | | $C$ | | | | |
|---|---|---|---|---|---|---|
| $G/C$ | $C_S$ | 3 | 4 | 5 | 6 | 7 |
| 0.35 | 0.4 | 3 | 4 | 5 | 6 | 7 |
| | 0.6 | 3 | 4 | 5 | 6 | 7 |
| | 0.8 | 3 | 4 | 5 | 6 | 7 |
| 0.5 | 0.4 | 2 | 3 | 4 | 4 | 5 |
| | 0.6 | 2 | 3 | 3 | 4 | 5 |
| | 0.8 | 3 | 3 | 4 | 4 | 5 |
| 0.65 | 0.4 | 1 | 2 | 2 | 3 | 3 |
| | 0.6 | 1 | 2 | 2 | 3 | 3 |
| | 0.8 | 1 | 2 | 2 | 3 | 3 |

(c) $c = 3$

| | | $C$ | | | | |
|---|---|---|---|---|---|---|
| $G/C$ | $C_S$ | 3 | 4 | 5 | 6 | 7 |
| 0.35 | 0.4 | 4 | 5 | 7 | 8 | 9 |
| | 0.6 | 4 | 5 | 6 | 7 | 8 |
| | 0.8 | 4 | 5 | 6 | 7 | 8 |
| 0.5 | 0.4 | 3 | 4 | 5 | 6 | 7 |
| | 0.6 | 3 | 4 | 4 | 5 | 6 |
| | 0.8 | 3 | 4 | 4 | 5 | 6 |
| 0.65 | 0.4 | 2 | 2 | 3 | 4 | 4 |
| | 0.6 | 2 | 2 | 3 | 3 | 4 |
| | 0.8 | 2 | 2 | 2 | 3 | 4 |

(d) $c = 4$

| | | $C$ | | | | |
|---|---|---|---|---|---|---|
| $G/C$ | $C_S$ | 3 | 4 | 5 | 6 | 7 |
| 0.35 | 0.4 | 5 | 7 | 8 | 10 | 11 |
| | 0.6 | 5 | 6 | 7 | 9 | 10 |
| | 0.8 | 5 | 6 | 7 | 8 | 9 |
| 0.5 | 0.4 | 4 | 5 | 6 | 7 | 8 |
| | 0.6 | 3 | 4 | 5 | 6 | 7 |
| | 0.8 | 3 | 4 | 5 | 6 | 7 |
| 0.65 | 0.4 | 2 | 3 | 4 | 4 | 5 |
| | 0.6 | 2 | 3 | 3 | 4 | 5 |
| | 0.8 | 2 | 2 | 3 | 3 | 4 |

# References


Bian, B., Pinedo, M., Zhu, N., Ma, S., 2019. Performance analysis of overtaking maneuvers at bus stops with tandem berths. Transportation Science. Advanced online publication 27 Mar 2019. https://doi.org/10.1287/trsc.2018.0841.

Bian, B., Zhu, N., Ling, S., Ma, S., 2015. Bus service time estimation model for a curbside bus stop. Transportation Research Part C: Emerging Technologies 57, 103–121.

Cortés, C. E., Burgos, V., Fernández, R., 2010. Modelling passengers, buses and stops in traffic microsimulation: review and extensions. Journal of Advanced Transportation 44 (2), 72–88.

Cvitanić, D., 2017. Joint impact of bus stop location and configuration on intersection performance. Promet-Traffic and Transportation 29 (4), 443–454.

Daganzo, C. F., 1994. The cell transmission model: A dynamic representation of highway traffic consistent with the hydrodynamic theory. Transportation Research Part B: Methodological 28 (4), 269–287.

David, H., Nagaraja, H., 2004. Order Statistics. John Wiley & Sons, Inc., New Jersey, USA.

Diab, E. I., El-Geneidy, A. M., 2015. The farside story: Measuring the benefits of bus stop location on transit performance. Transportation Research Record: Journal of the Transportation Research Board (2538), 1–10.

Fernández, R., 2010. Modelling public transport stops by microscopic simulation. Transportation Research Part C: Emerging Technologies 18 (6), 856–868.

Fernández, R., Burgos, V., Cortés, C. E., 2007. Results of the microscopic modelling of traffic interactions at stops, junctions and roads for the design of bus rapid transit facilities. In: European Transport Conference 2007, The Netherlands, October 2007.

Fernández, R., Del Campo, M., Swett, C., 2008. Data collection and calibration of passenger service time models for the transantiago system. In: European Transport Conference 2008, The Netherlands, October 2008.

Fernandez, R., Planzer, R., 2002. On the capacity of bus transit systems. Transport Reviews 22 (3), 267–293.

Fitzpatrick, K., Hall, K., Perdinson, D., Nowlin, L., 1996. Guidelines for the Location and Design of Bus Stops, Transit Cooperative Research Program Report 19. Transportation Research Board, Washington, D.C., USA.

Furth, P., SanClemente, J., 2006. Near side, far side, uphill, downhill: impact of bus stop location on bus delay. Transportation Research Record: Journal of the Transportation Research Board (1971), 66–73.

Ge, H., 2006. Traffic impacts of bus stops in urban area and related optimization techniques (in Chinese). Ph.D. thesis, Southeast University, China.

Gibson, J., 1996. Effects of a downstream signalised junction on the capacity of a multiple berth bus-stop. In: Proceedings of the 24th PTRC European Transport Forum, London.

Gibson, J., Baeza, I., Willumsen, L., 1989. Bus-stops, congestion and congested bus-stops. Traffic engineering and control 30 (6), 291–302.

Greene, W. H., 2003. Econometric Analysis. Pearson Education, New Jersey, USA.

Gross, D., Shortle, J. F., Thompson, J. M., Harris, C. M., 2008. Fundamentals of Queueing Theory, 4th Edition. John Wiley & Sons, Inc., New Jersey, USA.

Gu, W., 2012. Models of bus queueing at isolated bus stops. Ph.D. thesis, University of California, Berkeley, USA.

Gu, W., Cassidy, M. J., 2013. Maximizing bus discharge flows from multi-berth stops by regulating exit maneuvers. Transportation Research Part B: Methodological 56, 254–264.

Gu, W., Cassidy, M. J., Gayah, V. V., Ouyang, Y., 2013. Mitigating negative impacts of near-side bus stops on cars. Transportation Research Part B: Methodological 47, 42–56.

Gu, W., Cassidy, M. J., Li, Y., 2012. On the capacity of highway checkpoints: Models for unconventional configurations. Transportation Research Part B: Methodological 46 (10), 1308–1321.

Gu, W., Cassidy, M. J., Li, Y., 2015. Models of bus queueing at curbside stops. Transportation Science 49 (2), 204–212.

Gu, W., Gayah, V. V., Cassidy, M. J., Saade, N., 2014. On the impacts of bus stops near signalized intersections: Models of car and bus delays. Transportation Research Part B: Methodological 68, 123–140.

Gu, W., Li, Y., Cassidy, M. J., Griswold, J. B., 2011. On the capacity of isolated, curbside bus stops. Transportation Research Part B: Methodological 45 (4), 714–723.

Gupta, S. S., 1960. Order statistics from the gamma distribution. Technometrics 2 (2), 243–262.

Hisham, F., Bunker, J. M., Bhaskar, A., 2018. Development of a modified bus stop capacity model. In: Transportation Research Board Annual Meeting, 97th, Washington, D.C., USA.

Jaiswal, S., Bunker, J. M., Ferreira, L., 2010. The influence of platform walking on BRT station bus dwell time estimation. Journal of Transportation Engineering 136 (12), 1173–1179.

Kittelson & Associates, Inc., 2013. Transit Capacity and Quality of Service Manual, 3rd Edition. Transit Cooperative Research Program Report 165, Transportation Research Board, Washington, D.C., USA.

Larson, R. C., Odoni, A. R., 1981. Urban Operations Research. Prentice-Hall, New Jersey, USA.

Levinson, H., St. Jacques, K., 1998. Bus lane capacity revisited. Transportation Research Record: Journal of the Transportation Research Board (1618), 189–199.

Li, J., Gupta, S. D., Zhang, L., Zhou, K., Zhang, W., 2012. Evaluate bus emissions generated near far-side and near-side stops and potential reductions by ITS: An empirical study. Transportation Research Part D: Transport and Environment 17 (1), 73–77.

Menendez, M., 2006. An analysis of HOV lanes: Their impact on traffic. Ph.D. thesis, University of California, Berkeley, USA.

Newell, G. F., 1965. Approximation methods for queues with application to the fixed-cycle traffic light. SIAM Review 7 (2), 223–240.

Newell, G. F., 1982. Applications of Queueing Theory. Springer, Netherlands.

Newell, G. F., 1993. A simplified theory of kinematic waves in highway traffic, part II: Queueing at freeway bottlenecks. Transportation Research Part B: Methodological 27 (4), 289–303.

Nguyen, V. N., 2013. Bus prioritisation in motorcycle dependent cities. Ph.D. thesis, Darmstadt University of Technology, Germany.

Prescott, P., 1974. Variances and covariances of order statistics from the gamma distribution. Biometrika 61 (3), 607–613.

St. Jacques, K., Levinson, H. S., 1997. Operational analysis of bus lanes on arterials. Transit Cooperative Research Program Report 26, Transportation Research Board, Washington, D.C., USA.

Tan, H., Yang, X., 2014. A new capacity computing model of bus stop at upstream signalized intersection in peak. In: the 17th International IEEE Conference on Intelligent Transportation Systems.

Terry, D. S., Thomas, G. J., 1971. Farside bus stops are better. Traffic Engineering 41 (6), 21–29.

TRB, 2000. Highway Capacity Manual. Transportation Research Board, Washington, D.C., USA.

Vazquez-Leal, H., Castaneda-Sheissa, R., Filobello-Nino, U., Sarmiento-Reyes, A., Sanchez Orea, J., 2012. High accurate simple approximation of normal distribution integral. Mathematical problems in engineering 2012.

Wang, C., Ye, Z., Fricker, J. D., Zhang, Y., Ukkusuri, S. V., 2018. Bus capacity estimation using stochastic queuing models for isolated bus stops in china. Transportation Research Record: Journal of the Transportation Research Board. Advanced online publication. doi:10.1177/0361198118777358.

Wang, C., Ye, Z., Wang, Y., Xu, Y., Wang, W., 2016. Modeling bus dwell time and time lost serving stop in china. Journal of Public Transportation 19 (3), 55–77.

Whitt, W., 1993. Approximations for the GI/G/m queue. Production and Operations Management 2 (2), 114–161.

Zhao, X., Gao, Z., Jia, B., 2007. The capacity drop caused by the combined effect of the intersection and the bus stop in a CA model. Physica A: Statistical Mechanics and its Applications 385 (2), 645–658.